UNIVERSIDADE DE LISBOA
FACULDADE DE CIÊNCIAS
DEPARTAMENTO DE BIOLOGIA ANIMAL

Mapping seagrass meadows, using low altitude aerial images

Mestrado em Ecologia Marinha

ROBERT COMAS GONZALEZ

Dissertação orientada por:
Professor Doutor Francisco Andrade (Departamento de Biologia Animal – Centro de Oceanografia)

2015

ACKNOWLEDGMENTS

I would like to thanks Francisco Andrade for his teachings and motivation not only as my supervisor in this project but also as a professor in my Master degree.
Thanks also to my colleague Rui Cereja, for joining me in the field work and his always predisposition to help, and to the *Laboratório Marítimo da Guia* for the logistical support to conduct the thesis.

Gratitude to all people contributing to the freedom of knowledge such as developing free softwares and low cost methodologies, a growing need to combat the will of limiting the knowledge distribution.

Many thanks to Rui Monteiro for being my secretary and portuguese translator during the whole Master program.

Thanks to Carmen and Fernando for welcoming and feeding me during several times along the present study time-line.

Special thanks to my parents for their unfaltering support along all steps in my life.

To Carla, for her help, patience, encouragement and love.

RESUMO

As pradarias de ervas marinhas, assim como muitos outros ecossistemas marinhos, estão a sofrer uma degradação sem precedentes em todo o planeta. Devido à rápida perda destes habitats, são necessárias técnicas de monitorização que permitam de forma precisa caracterizar o estado das pradarias de ervas marinhas ao longo do tempo. Adicionalmente é importante considerar o custo e logística na monitorização, assim como a sua flexibilidade em diferentes condições de amostragem e de forma não intrusiva, para um trabalho de campo periódico. Varias metodologias tem sido propostas ao longo do tempo para o estudo de ecossistemas marinhos como as pradarias de ervas marinhas.
O objectivo do presente trabalho é o desenvolvimento e teste (análise comparativa) de uma nova abordagem de baixo custo, ao mapeamento dos limites e densidade de pradarias de ervas marinhas, com recurso a imagens aéreas a baixa altitude e alta definição (0.1 m), obtidas autonomamente. Pretendeu-se assim vencer várias das limitações propostas por metodologias anteriores. Foram abrangidos 3 níveis na análise comparativa: as fases de aquisição (metodologia), a avaliação da influência das condições de aquisição das mesmas e a classificação das imagens. A análise comparativa dos diferentes resultados foi dirigida, não só à avaliação da expressão territorial das manchas – extensão e delimitação – mas também à avaliação comparativa, em termos de resultados e exequibilidade, das metodologias empregues.

O trabalho de campo foi desenvolvido na península de Tróia, tendo como alvo duas áreas principais: uma no extremo NO da península de Tróia e outra entre as instalações da Marinha e o novo cais dos ferries.

Para a análise comparativa ao nível da aquisição das imagens, a pradaria situada no extremo NO da península de Tróia, foi monitorizada com uma metodologia já testada e avaliada em prévios estudos, a partir de imagens oblíquas em cor verdadeira, obtidas a partir de um ponto fixo elevado na proximidade (o topo de um dos hotéis existentes). Por outro lado na pradaria situada na localização do novo cais dos ferries, foi aplicada a nova metodologia proposta, com fotografia a partir de um balão cativo, a uma altitude de aproximadamente 50 m, que foi guiado ao longo da linha de costa por um operador.

Vários fatores ambientais foram inicialmente considerados para o teste das metodologias:

vento, ondas, maré, etc. Sendo que o nível de maré foi o fator finalmente usado para a análise comparativa consoante as condições de aquisição. Os levantamentos fotográficos de ambas as manchas foram realizadas com uma periodicidade de base mensal, sempre em condições de baixa-mar de águas vivas. O nível de maré abrange um amplo intervalo de possibilidades, contudo, as imagens foram diferenciadas em dois grupos no contexto das condições de aquisição: emerso e submerso. Emerso refere-se a imagens em que a pradaria apresenta alguma porção emersa e submerso, refere-se às imagens com a totalidade da pradaria submersa. Assim, estes dois grupos permitiram uma clara diferenciação entre diferentes condições ambientais flutuantes e típicas dos ambientes estudados. Estas condições foram também condicionantes para a aquisição de imagens aéreas com ambas as metodologias, o que permitia avaliar a flexibilidade da aplicação da nova metodologia proposta.

Em ambos as metodologias de aquisição, as imagens originais em cor verdadeira foram ortorrectificadas (georreferenciadas), com base em levantamentos de campo levados a cabo com recurso a um sistema de GPS com correcção diferencial RTK, para obter os pontos de controlo de referencia para o processo.
No caso das imagens obtidas com a nova metodologia proposta, a partir do balão, foram agrupadas 2 ou 3 imagens, em mosaicos representativos de uma secção significativa da área alvo.

Finalmente, estas imagens rectificadas e em cor verdadeira, foram processadas para permitir avaliar a distribuição e densidade das manchas de ervas marinhas. Para a análise comparativa ao nível de classificação da imagem, foram utilizados e comparados diferentes algoritmos de classificação, nomeadamente classificação de base pixel e classificação baseada em objectos. Todas as imagens classificadas foram reclassificadas até obter mapas binários representando as classes: Ervas marinhas; Não-ervas marinhas.

A partir dos mapas binários para cada uma das imagens processadas, foram obtidos: área da classe Ervas marinhas; precisão de classificação da imagem (a través da comparação com pontos controlo na imagem em cor verdadeira); e o coeficiente kappa (comparando mapas binários). Estes parâmetros foram usados no contexto da análise comparativa para os 3 níveis propostos:

- As áreas da classe Ervas marinhas foram comparadas para testar a semelhança/diferença entre a área de cobertura em cada uma das condições de

amostragem (emerso/submerso) para cada uma das metodologias usadas (imagens obliquas/imagens com o balão). Assim, foi possível comparar se a situação de maré, influía nos resultados de estudos de densidade e distribuição a través das imagens aéreas.

- A precisão na classificação das imagens foi comparado para cada um dos 3 níveis, por forma a avaliar semelhanças/diferenças entre o processo de aquisição das imagens (metodologias), entre condições de amostragem e entre abordagens nas classificações das imagens.

- O coeficiente kappa foi obtido a partir da comparação entre mapas binários, comparando condições de amostragem (emerso/submerso) e classificação da imagem (pixel/objecto).

Os resultados mostraram que as imagens obtidas com o balão apresentavam menos erros e distorções no processo de rectificação, devido a sua maior verticalidade. Contudo, tinham a limitação decorrente de uma distribuição mais limitante dos pontos de controlo de referencia obtidos com o GPS-RTK. As imagens obtidas a partir do balão a 50 m de altitude permitiram abranger a largura toda da pradaria.
Por outro lado, os resultados obtidos através da análise das imagens classificadas (mapas binários), mostraram diferencias significativas (p=3.221×10^{-05}) só ao nível de comparação entre abordagens de classificação das imagens, sendo que a classificação baseada em objectos, ofereceu resultados mais precisos que a classificação de base pixel.

Este estudo demonstrou que a metodologia proposta, com o balão cativo, oferece a possibilidade de mapeamento de pradarias de ervas marinhas a baixo custo, com imagens de alta resolução e com elevada precisão. Os resultados a nível de precisão na nova metodologia usada foram semelhantes aos obtidos com a metodologia comparada de imagens obliquas, já demonstrada em estudos anteriores como uma metodologia que vencia limitações de outras abordagens. As maiores limitações para à aplicação da nova metodologia com o balão cativo foram devido as condições meteorológicas, nomeadamente o vento. Contudo, a nova metodologia com o balão ofereceu outras vantagens relativamente às fotografias obliquas além do menor error na rectificação: nomeadamente, a independência de aplicação e o maior detalhe das imagens para representar a complexidade dos ecossistemas.
No contexto das condições de amostragem, foi demonstrado que o nível de maré não é um

fator que influencie resultados e interpretações, desde que dentro de um limite de visibilidade mínima e para uma cota de maré máxima de 0.8 m, para permitir obter imagens desejáveis. Finalmente, a maior precisão obtida com a classificação baseada em objectos indica que este abordagem oferece uma maior capacidade para classificar as imagens destes sistemas aquáticos superando possíveis limitações p. ex., de visibilidade devida à turbidez o à presença de objectos não desejados na classificação.

Este estudo demonstrou a possibilidade e interesse do mapeamento não intrusivo, de baixo custo e com elevada precisão de pradarias de ervas marinhas, mas que também pode ser aplicado noutros ecossistemas intertidais, oferecendo uma nova ferramenta para à necessária monitorização periódica de sistemas complexos.

ABSTRACT

Seagrass meadows, together with other coastal marine habitats, are facing unprecedented declines, which requires low cost methodologies for its highly frequent periodic monitoring, able to represent accurately the complexity of those ecosystems. In this context, the aim of the present study was to develop a new approach using nadir aerial photographies from low altitude – high resolution (0.1 m), with a helium balloon system. The methodology was tested (comparative analysis) at 3 levels. First, at methodology level agains an oblique terrestrial photography methodology used in previous studies at the same location. Second, at sampling conditions level for typical changing environment situations – emerged and submerged. Third, at image classification level comparing pixel- and object-based classification. Testing for each of the levels, was through the analysis of processed images taken, which include: georeferencing and, for nadir aerial photographies, a mosaicking process, and image classification. Final images data, were obtained from the binary (seagrass / non-seagrass) classified maps of each treated image, from which it was obtained: area of seagrass class for each image; classification accuracy; and kappa coefficients values from comparison between classified maps. Hence, area results were used to test for sampling conditions comparative analysis; classification accuracies were used to test for 3 levels (methodology, sampling conditions and image classification) comparative analysis; and kappa analysis to compare binary maps between pairs of images for sampling conditions and image classification comparative analysis. Results showed significance differences only at image classification level comparison (p=3.221×10^{-05}), scoring higher accuracy values for object-based classification. The study demonstrated that highly accurate results can be obtained through the proposed low cost methodology, for different sampling conditions, overcoming some classification issues with the object-based approach. Thus, allowing to reliably represent the seagrass meadows structural complexity through low altitude-high resolution images in a non-intrusive low-cost approach.

Keywords: seagrass meadows, low-cost, nadir aerial photography, helium balloon, georectification, mosaicking, pixel- and object-based classification.

TABLE OF CONTENTS

1 INTRODUCTION

Seagrass meadows are critical components of coastal and estuarine ecosystems. They influence local coastal biogeochemistry through many features and processes (Marbà et al., 2006). For instance, the seagrass canopy influences sediment deposition (Gacia et al., 1999) and stabilizes the substrate (Fonseca and Bell, 1998; Silveira et al., 2011). More over, those habitats, are important coastal primary producers (Duarte and Chiscano, 1999) and are used as nursery by many species (Heck et al., 2003). Seagrass beds are dynamic habitats that naturally change over time and space (Duarte et al., 2006; Frederiksen et al., 2004). Nonetheless, this dynamics seems to be unnaturally tending towards a global decrease in their density and distribution (Orth et al., 2006; Waycott et al., 2009). In Portugal, seagrass populations are suffering an unprecedented decline in size and distribution (Cunha et al., 2013). This fact, together with the ecological importance of those habitats, justifies the relevance of their monitoring. Moreover, those concerns, lead to the development of new sampling approaches, allowing researchers to periodically and accurately analyze the habitats with easy and low cost methodologies.

Study of seagrass meadows and other benthic habitats, can be conducted using several methodologies. In situ survey samplings, including diving transects, has been widely applied (Duarte and Kirkman, 2001). However, for a short-term repetitive sampling purpose, those techniques may be logistically unviable and economically expensive (Dekker et al., 2006). Furthermore, those methodologies involve a high degree of habitat intrusiveness, especially when periodic samplings are needed.

The large variety of digital imagery approaches, offers nowadays a good choice to solve those issues, allowing for the measurement of parameters such as coverage and involving different methodologies with accurate results (Gillespie et al., 2008; Hill et al., 2014; Kutser et al., 2007).

Information from the reality captured with a digital photograph, consists of a matrix created by the sensor, composed by X columns and Y rows. Each image coordinate (XY), represents the spectral response of the radiation reflected from the captured scene and is the smallest unit of the digital image, called pixel. Each pixel presents one color, creating the visual image as a raster file (grid of pixels). These captured values, can be therefore processed and analyzed to

highlight and extract information from objects (natural or artificial) represented by a certain quantity and distribution of pixels – a digital image.
Therefore, seagrass beds, with dense canopies with specific optical properties, can be mapped and analyzed by extracting the corresponding spectral information from the original image (Dekker et al., 2006; Silva et al., 2008; Zimmerman and Dekker, 2006).

The results of digital images analysis, goes tie to the acquisition process as well as their following processing.
Satellite imagery is a remote methodology, widely used for landscapes monitoring. This approach has been proved as an accurate methodology to study shallow marine habitats including seagrasses (Lyons et al., 2012; Phinn et al., 2008; Roelfsema et al., 2014). Still, it suffers from both spatial and time resolution limitations due to the available ground resolutions and periodicity of revisit of the platform (Andrade and Ferreira, 2011; Boyle et al., 2014). Indeed, whenever some features of the satellite imagery improve, it usually is against the sacrifice of others (e.g. spectral resolution versus temporal resolution) (Nagendra and Rocchini, 2008). Even more, in complex Geographic Information System (GIS) analysis of satellite imagery, accuracy of time-change studies is difficult to assess because of the large number of variables associated with the process (Macleod and Congalton, 1998).
Airborne imagery, together with GIS data, has been successfully used as an alternative to satellite imagery, to provide low altitude aerial images of seagrass meadows (Hovel and Lipcius, 2001; Su et al., 2006; Zharikov et al., 2005). This methodology, can overcome many of the satellite limitations commented, offering features such as high resolution images (<1m), not limited by cloud conditions and with less timeline limitations (Dekker et al., 2006).
Furthermore, many researches have recently chosen the use of drones, a growing trend for ecological studies through large-scale imagery. Nowadays drones can provide an advantage over the airborne, regarding their cost-effectiveness (Koh and Wich, 2012), especially when used to carry out field work with frequent periodicity. However, the autonomy and integrity of the drone is still a concern to consider, when mapping water surfaces during long time-lapse (> 45 min).
Andrade and Ferreira, 2011, developed and tested a new methodology using terrestrial oblique large-scale photography for monitoring shallow seagrass meadows. This low cost methodology, clearly covered most of the limitations found in other sampling techniques previously referred. However, as the authors concluded, factors such us turbidity, drifting material, physical obstacles, image obliquity, camera-target distance, or even the vertical plant

position due to the depth-plant height relation, can influence the results.

Besides the multiple possibilities of the acquisition methodologies and strategies, subsequent image processing can be performed using a variety of image processing tools, some, with prohibitive licensing costs, while others offer free softwares for remote sensing and GIS research with a wide user support (Neteler et al., 2012).
Image processing involves a variety of techniques, settings and steps, that clearly condition the results and interpretations of the analysis. Thus, image processing *per se* can help to fix or deal with acquisition limitations like the ones reported by Andrade and Ferreira, 2011.

Considering all issues above, a new low cost, user-friendly and non-intrusive methodology is proposed – including all corresponding steps – to obtain and analyze low altitude vertical/nadir aerial images, to avoid or minimize some of the above mentioned limitations as well as to optimize some processes and future field work decisions.

Objective

The aim of this research, is to develop a new approach to mapping the density and distribution of seagrass meadows, using true color low altitude aerial images. The new proposed approach is tested (comparative analysis) in three principal steps (levels) through the analysis of images taken and processed:

- Image acquisition (methodology): can the new image acquisition approach overcome other image acquisition approaches issues?
- Sampling conditions: have field sampling conditions influence in the image analysis?
- Image classification: can the image classification approach contribute to overcome seagrass mapping issues in the different sampling conditions and image acquisition approach?

2 MATERIAL AND METHODS

2.1 Study site

The present study was conducted on 2 seagrass meadows at Tróia peninsula, an elongate sandbank with SE-NW orientation at the mouth of the Sado estuary, Portugal (Fig. 1).

Estuarine inlet channels are influenced by strong coastal dynamism. This dynamism is unsuitable for seagrass colonization. Indeed, bordering the north tip coastline of the Troia peninsula, sandy bottoms dominate the shallow underwater landscape. However, an almost continuous seagrass meadow is located at the NW tip of the peninsula (Fig. 1: seagrass meadow 1) – 38º 29' 31"N; 8º 54' 31"W. At this location, the stable bay-shaped area, provides favorable conditions for the seagrass meadow to growth (Andrade and Ferreira, 2011; Silveira et al., 2011).
Following the estuarine border of the Troia peninsula upstream, about 4 km to the SE, another seagrass meadow is located between the NATO military facility and the new ferry boat jetty (Fig. 1: seagrass meadow 2) – 38°28'9.86"N; 8°52'0.19"W.

Both meadows, extending at the intertidal and shallow subtidal, are dominated mainly by *Zostera marina* and *Zostera noltii* (Cunha et al., 2013, 2009).

2.2 Images acquisition

Sites close to each other can be under different abiotic conditions influencing biotic distribution and composition. The presence of the seagrass meadows surrounded by a sandy landscape on the study locations are such an example (Silveira et al., 2011). Nevertheless, our survey areas are under similar daily conditions regarding aerial imagery acquisition. Together with their similar biotic composition relevant for the image analysis process (*Zostera* spp.), and in view of our study goals, focused on the imagery methodology *per se*, this allowed us to consider them as two sampling sites from the same location.
Thus, each study site was object of one specific methodology to carry out the comparative analysis at methodology level. This decision offered the main benefit of avoiding interferences

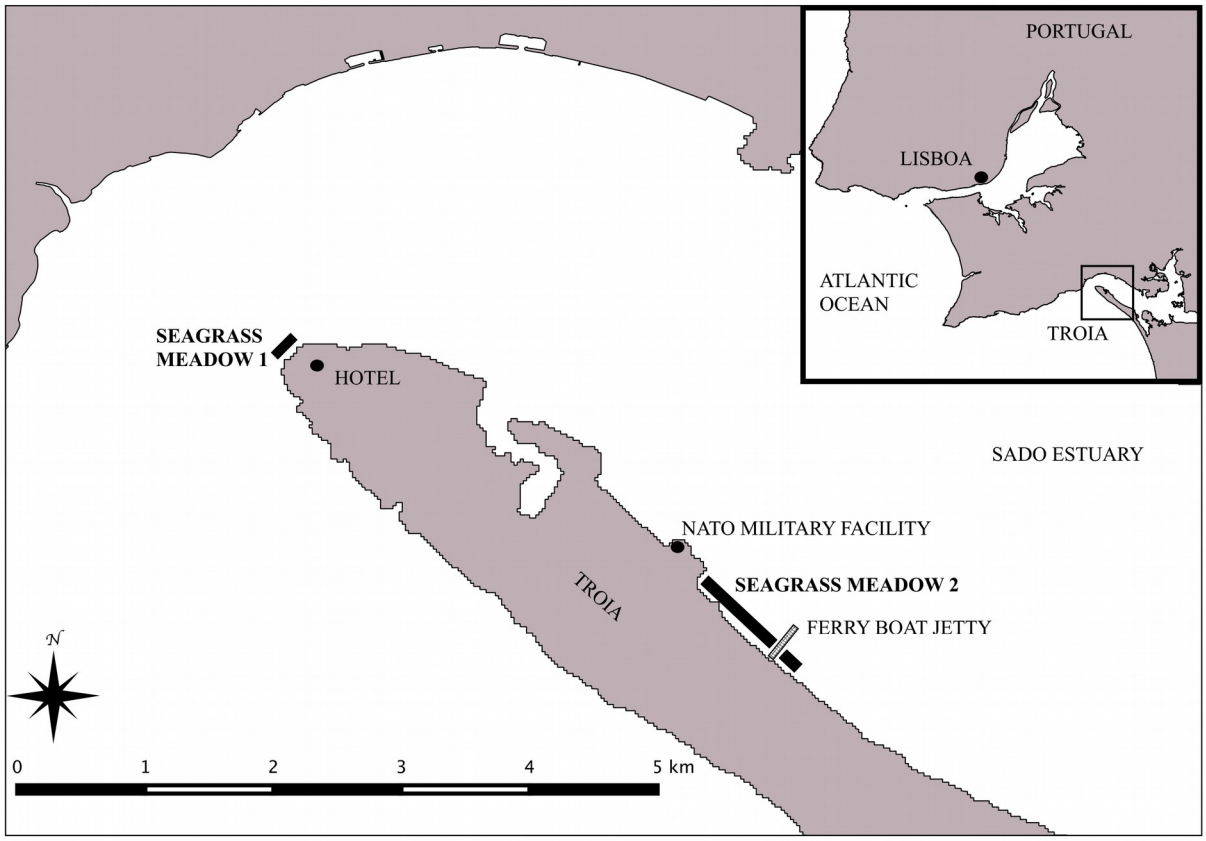

Fig. 1 Study locations: seagrass meadow 1 and seagrass meadow 2 in the lower Sado estuary.

between the approaches, as described bellow, manly regarding the water column visibility during sampling procedures.

Schemes in Fig. 2 and 3 represents the process steps for each methodology, from image acquisition to image processing and analysis.

2.2.1 Oblique terrestrial photography

Seagrass meadow 1 (Fig. 1) was photographed using the oblique terrestrial photography method (OTP) described by Andrade and Ferreira, 2011 for the same location, with accurate results for the seagrass mapping and overcoming most of the issues of other methodologies.

Images of the meadow were taken from a fixed altitude – 39 m above mean sea level (MSL) – at a fixed point on the highest floor of a nearby hotel, from where it is possible to see the entire meadow surface with no visual obstruction (e.g., Fig. 4, *a* and *b*). The observation point had a distance to the meadow ranging from ~250 m (to the closest point) to ~450 m (to the

farthest point). A tripod was used to stabilize and ensure, the exact same camera position for all image sets from this location. Fixed and permanent buildings from the opposite estuary margin were used as references to ensure the same framing was used in every campaign.

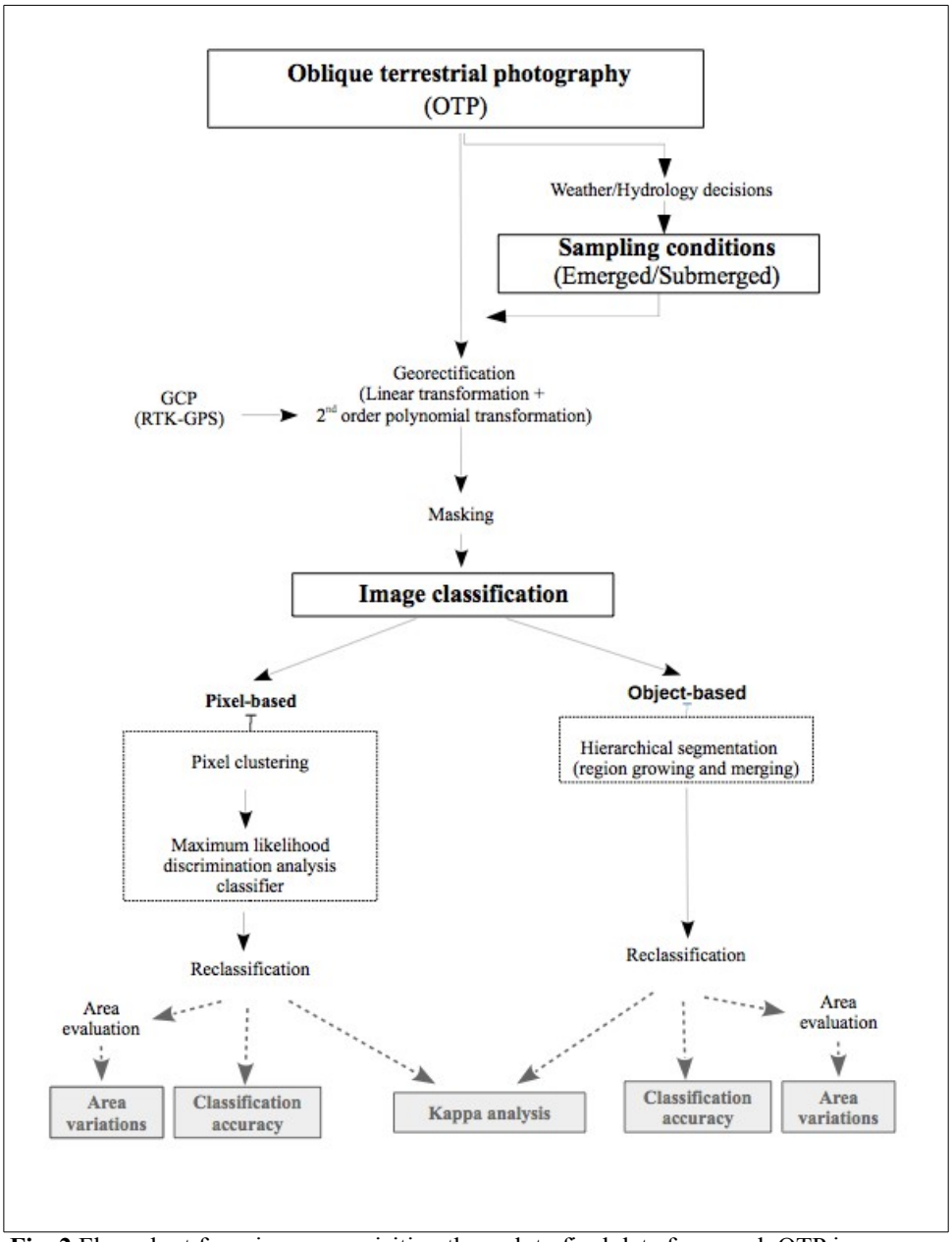

Fig. 2 Flow chart from image acquisition through to final data from each OTP image (seagrass coverage) and its analysis and validation (area variations, classification accuracies and kappa) analysis).

Camera used was a Nikon D90 with a Nikkor 18-55 mm lens set to a fixed 34 mm focal length allowing to frame the whole meadow. A 52 mm circular polarizer filter was attached to minimize light reflections over the water covering the meadow.

The camera was set to shutter priority mode (S), with a shooting speed of 1/125", -1/3 exposure compensation (EV) and ISO 200. Images obtained were true color RGB 24bit/pixel, 4288 columns × 2848 rows.
Finally, a timer remote shooter release was set in order to automatize the shooting process every 2 minutes. In each session, an average of 90 images were taken from the end of ebbing tide, through slack water and into early flood, thus covering the lowest tide period.

OTP images were taken from the hotel every spring tide, whenever weather conditions allowed from October 2014 through August 2015.

2.2.2 Nadir aerial photography

Seagrass meadow 2 (Fig. 1), was photographed using the new proposed nadir aerial photography (NAP) approach.
This methodology, involves a camera attached to a tethered-helium balloon taking low altitude aerial images. The prototype of this setup consist of a latex balloon, filled with helium to a diameter of ~1.5 m (Fig. 5, *a*). The camera, on a waterproof case, was attached to the balloon (Fig. 5, *b*). This case, worked as both the suspension platform and as a protection, against eventual balloon failures considering their integrity lifetime of 4 -5 uses, and weather eventualities.

The whole balloon and platform mounting (Fig. 6), was developed in a low-cost and user-friendly perspective.
The wire connecting the balloon to the rest of the setup, was self-interlaced, at a certain level, to allow for the balloon release from the setup (namely the camera) in case of an unexpected strong wind raft. Below, the proposed attaching mechanism with the elastic gums, acting as a subjection and damping vertical movements. An important remark for the tether setup, was to ensure the horizontality of the camera to allow for as vertical images as possible.
To reduce the rotational movement of the camera, a metal swivel was used to connect the elastic

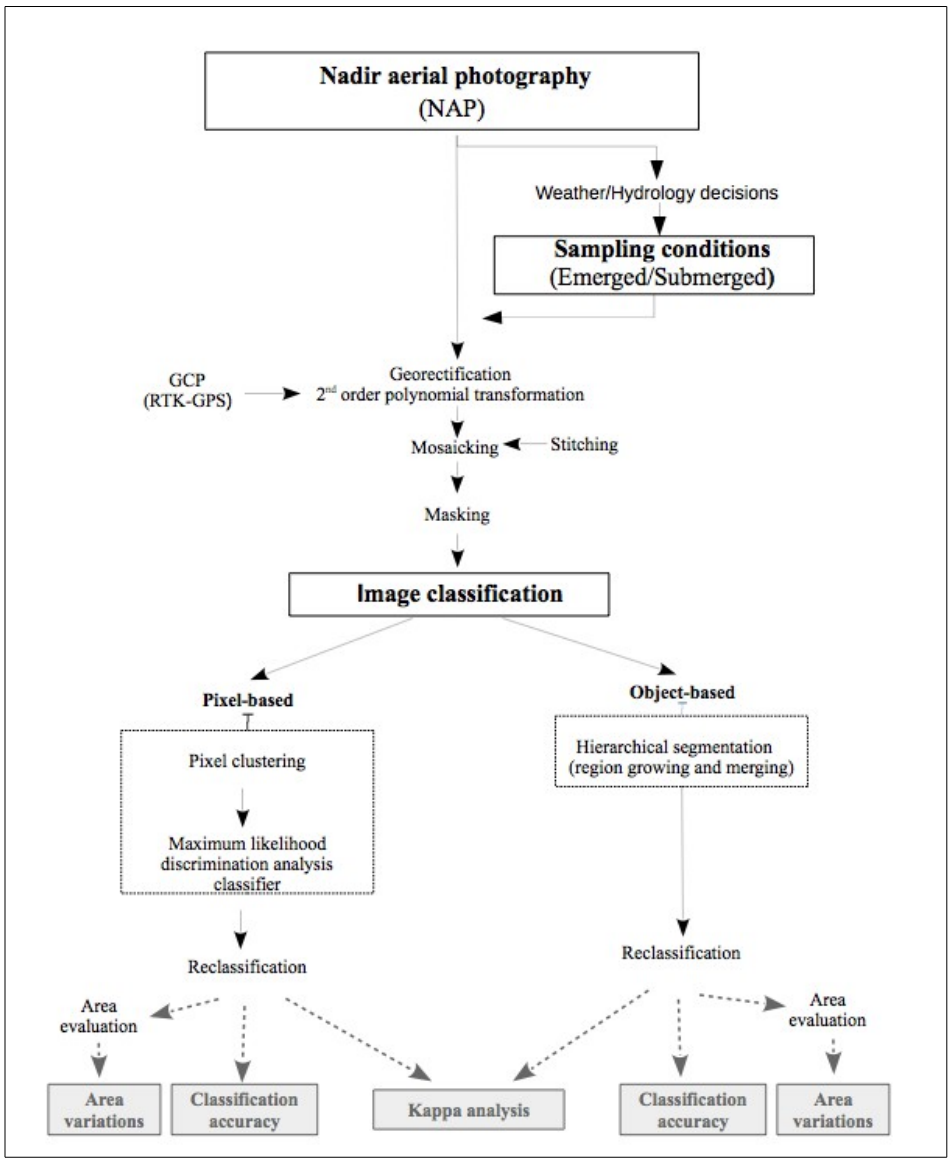

Fig. 3 Flow chart from image acquisition through to final data from each OTP image (seagrass coverage) and its analysis and validation (area variations, classification accuracies and kappa) analysis).

and lines system to the balloon attachment. This allowed some rotational independence from the balloon decreasing its movement influence on the camera. Furthermore, a wing made of polystyrene to enable a large surface with low additional extra weight, was designed to be mounted/unmounted easily with elastic gums over the case. This wing reduced the rotational movement from 360º to ≤ 90º.

Fig. 4 Examples of original photos taken with OTP, from the hotel (*a,b*) and NAP, from the balloon (*c,d*).

The camera used for this methodology was a Canon Powershot S110 with a 5.20 – 26 mm lens. The camera, together with the Canon Waterproof Case WP-DC47 used, had a total weight of 650 g, making it able to be lift by the balloon that allowed a maximum weight lifting of c. 1.5 kg. Several field tests were conducted to get the best camera settings, combined with the 50 m altitude mentioned above. Finally, the camera was set to the minimum focal length, 5.20 mm; shutter priority mode (Tv); 1/500 s shooting speed; -1/3 EV and ISO 320. This settings combination, proved to be a good option to cover a wide range of atmospheric light variations (manly due to clouds), to optimize the underwater objects contrast and to avoid blurred images. Images obtained were true color RGB 24bit/pixel, 4000 columns × 3000 rows.

Finally, time lapse was set through Canon Hack Development Kid (CHDK), version 1.3.0. This free software, once installed in the camera, allows for multiple extra-functions (CHDK, 2007). Different shooting intervals were tested, with an optimum range at 10 s. This time

lapse, allowed for covering the whole meadow with an overlapping between contiguous images (Bendell and Wan, 2011; Grenzdörffer et al., 2008).

Fig. 5 Balloon filling process (a) and camera with waterproof case and tether system (b).

The whole mechanism was attached to a Dyneema tether line payed out from a fishing rod. Initial tests were carried to determine the best operational altitude, with a value of c. 50 m having been selected (this is a theoretical value measured from the total fishing line length launched). From this altitude it was possible to frame the complete meadow width, considering the minimum 5.20 mm focal length allowed for the camera settings. Higher altitudes gave unnecessary destabilizations, and lower did not guarantee the whole wide meadow capture.

The balloon was guided for photographing the whole meadow width, along its entire length during spring tides.
During each photo survey with the balloon system, color cards were used to signpost and differentiate some possible confusing spots of seagrass / not seagrass.

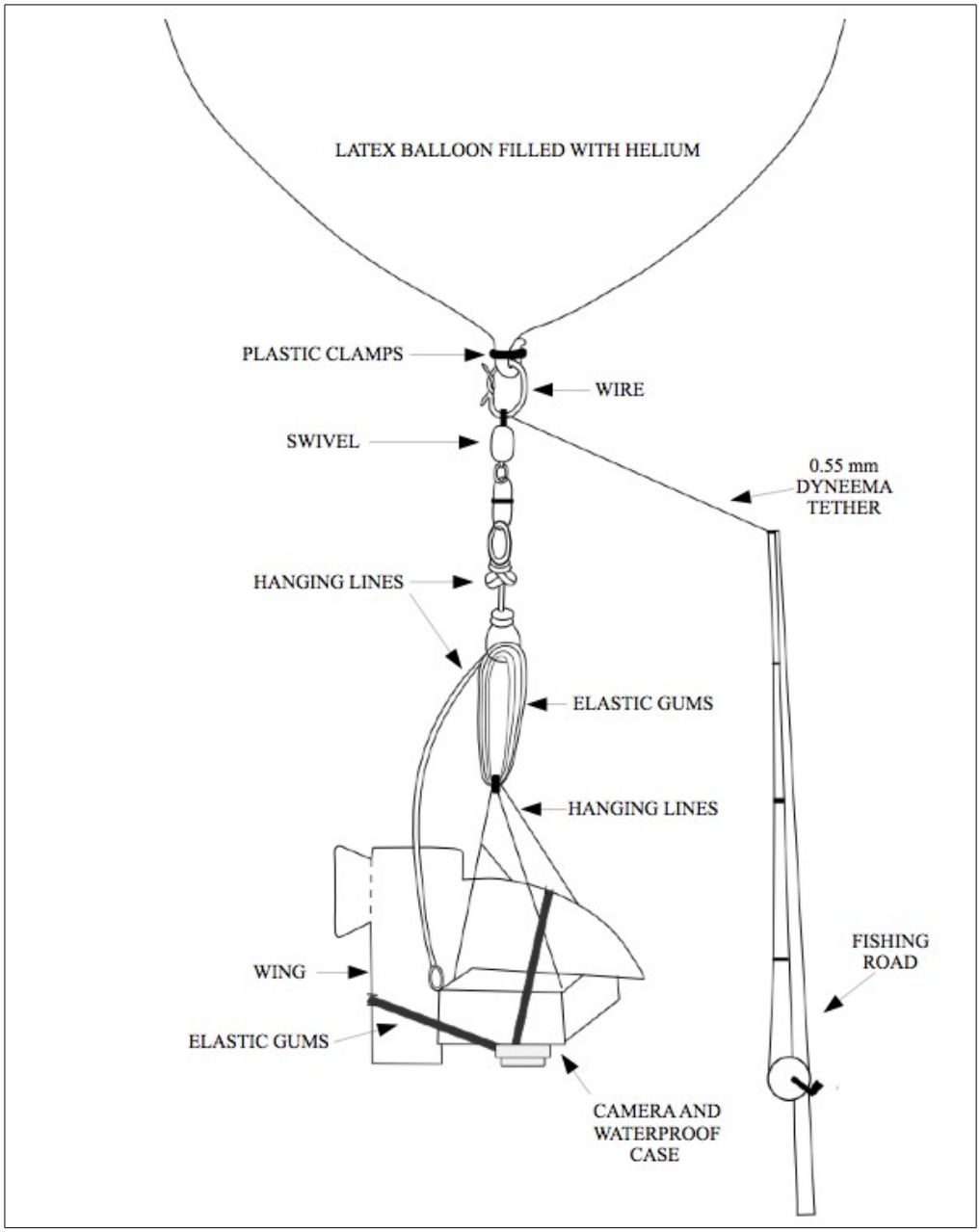

Fig. 6 Balloon mounting system with each structural part described.

The meadow was photographed from October 2014 to August 2015, whenever tide and weather conditions allowed. Usually, during each survey, it was possible to repeat the process 2 to 3 times, with an average of 200 images per path (total meadow length).

2.3 Sampling conditions

Aerial images quality of submerged habitats is fully dependent on local hydrological dynamism and weather conditions (Klemas, 2013). Many variables (e.g. wind, waves or tidal coefficient) and their multiple interactions make it virtually impossible to predict water column visibility in the estuary (Doxaran et al., 2009). Specially, multi-temporal scale effects on the estuarine turbidity, such as river run-off (Fabricius et al., 2013), make it unfeasible to incorporate such a prediction onto the daily or weekly field duties decisions. Additionally, random anthropogenic activity, over or close to the meadows, often lifts bottom sediments. Nonetheless, sampling strategy was deployed taken in consideration limiting conditions easily and daily predictable through public tide charts (IH, 2015, 2014) and forecast web sites (Hornik, 2015).

Commonly on both OTP and NAP methodologies, tide was the most limiting variable to consider. Inside the Sado estuary, tides vary in range from ~1m during neap tides to ≥ 3.5 during spring tides (IH, 2015, 2014).
As mentioned before, only spring tide periods were considered for sampling. This decision was taken given previous field experiences that proved a maximum tide level of ~0.8 m, to allow for desirable low altitude seagrass images. Variations of monthly tide behavior, allowed for different windows of opportunity for the field surveys, with a maximum of +/- 5 days from the lowest tide prediction.

Wind was the second main limiting variable. Deployment of the helium balloon, as suggested by other authors using similar approaches (Baker et al., 2004; Kawamura et al., 2011; Lonneville et al., 2014, 2013), can be safely achieved at wind speeds ≤ 5 knots. OTP, on the other side, did not have this limitation. However, winds > 10 knots, very often (depending on wind direction) produced a rough water surface, making it impossible to see the submerged part of the meadow.

Other variables (mainly related to the light radiation) such as clouds, solar time or season, were obviated considering the two main limiting variables above. Still, light radiation differences between sampling seasons were efficiently overcome with camera settings in both methods.

Images selection for comparative analysis

From both wind and tide, wind was not a factor to consider for the comparative analysis since it did not induce differences in terms of seagrass image acquisitions besides its limiting ranges. On the other hand, tide, as Andrade and Ferreira, 2011 concluded, could be an issue for mapping the seagrass meadow limits considering depth-leaf position relations and meadow visibility. In order to perform the comparative analysis for sampling conditions, 2 characteristic sampling conditions were considered:

- Emerged: images with some emerged portion of the meadow (Fig. 4, *a* and *c*) and taken at the lowest tide time (with a maximum difference of +10 minutes) between ~0.2 and ~0.4 m from the hydrographic zero (HZ) depending on the sampling date (Tables 1 and 2).

- Submerged: images with the whole meadow submerged (Fig. 4, *b* and *d*) taken during the incoming between approximately +30 and +80 minutes from the lowest tide (Tables 1 and 2).

From emerged to submerged, a wide range of tide level can be found, which can lead to different interpretation of the seagrass density and distribution through the images taken, considering the randomness of seagrass leafs position (Koch et al., 2006) and the constant changing clarity of the estuarine water (Fabricius et al., 2013). Nonetheless, and considering the limit of ~0.8 m HZ tide level, the proposed groups offered a clear and representative range to test the image acquisition of the seagrass meadow in two differentiated and characteristic sampling conditions: emerged and submerged.

The differentiate sampling conditions (emerged/submerged) were considered for both OTP and NAP methodologies.
OTP images, having less wind limitations, offered the possibility to obtain images of emerged and submerged conditions from the same survey at most, with a 1 day difference (Table 1). NAP images on the other side, were more limited to combine both optimal tide and wind conditions. Even when it was possible to fly the balloon, it was not possible to operate for such wide tide ranges as from the hotel. Therefore, for the NAP approach, selected images for different conditions, span a time interval of up to 44 days (Table 2).

Images selection, was based on the best quality of the seagrasses view. Still, some turbidity

over the meadow was accepted to allow for the analysis considering the timeline limitations. Four pairs of OTP and NAP images were selected representing emerged and submerged conditions. Each image of each pair, corresponding to a different sampling condition from same location and temporally close from its couple (same shading color in Tables 1 and 2).

Table 1 Data for the final OTP selected pictures: Date; Image; Condition: sampling conditions; T: time (universal time, UT) of image acquisition; T, h tide: time (UT) and low tide level (HZ) predicted by the IH chart (IH, 2015, 2014); C: tide coefficient, Wind and Clouds predicted by Windguru website forecast (Hornik, 2015).

Date (dd/mm/yy)	Image	Condition	T	T , h tide	C (%)	Wind (kts)	Clouds (%)
23/12/14	OTP1	Emerged	09:47	09:39, 0.4	98	6	13
24/12/14	OTP2	Submerged	11:34	10:24, 0.4	95	5	0
21/01/15	OTP3	Emerged	09:24	09:26, 0.3	107	13	0
21/01/15	OTP4	Submerged	10:48	09:26, 0.3	107	8	0
19/02/15	OTP5	Emerged	09:11	09:09, 0.2	115	10	0
19/02/15	OTP6	Submerged	10:29	09:09, 0.2	115	11	0
20/04/15	OTP7	Emerged	10:49	10:48, 0.3	100	4	99
20/04/15	OTP8	Submerged	11:59	10:48, 0.3	100	4	99

Table 2 Data for the final NAP selected pictures: Date; Image; Condition: sampling conditions; T: time (universal time, UT) of image acquisition; T, h tide: time (UT) and low tide level (HZ) predicted by the IH chart (IH, 2015); C: tide coefficient, Wind and Clouds predicted by Windguru website forecast (Hornik, 2015).

Date (dd/mm/yy)	Image	Condition	T	T , h tide	C (%)	Wind (kts)	Clouds (%)
18/05/15	NAP1	Emerged	08:42	08:44, 0.4	97	1	100
01/07/15	NAP2	Submerged	08:36	08:09, 0.7	88	3	100
18/05/15	NAP3	Emerged	08:40	08:44, 0.4	97	1	100
01/07/15	NAP4	Submerged	08:39	08:09, 0.7	88	3	100
18/05/15	NAP5	Emerged	08:37	08:44, 0.4	97	1	100
01/07/15	NAP6	Submerged	08:41	08:09, 0.7	88	3	100
18/05/15	NAP7	Emerged	08:34	08:44, 0.4	97	1	100
01/07/15	NAP8	Submerged	08:45	08:09, 0.7	88	3	100

2.4 Images georegistration

Images were geometrically corrected throughout a rectification process (georectification). This is a correction of remotely sensed data through a transformation function defined by ground control points (GCP) (Rocchini et al., 2011). GCPs are recognizable points both in the field, were the coordinate (X/Y) are read, and in the image, were their position (columns/lines) are read and selected. Thus, the transformation is performed from the image referential column/line to the coordinate referential X/Y.
Georectification allows from transforming an oblique to a vertical view of the image target (orthogonalization), to obtain the same geometric resolution throughout the whole target surface which now will have coordinates (georeferenced). Thus, allows for areal quantification of classifications information. Application of this process, to all images, requires a first step of GCP sampling followed by the computational transformation process or georectification. Computational operations of all images, were conducted using free GIS and image processing softwares: GRASS GIS version 7.0.0 (GRASS, 2015) and Quantum GIS (QGIS) version 2.8.1 – Wien (QGIS, 2009).

2.4.1 OTP images

Seagrass meadow images presented an obliquity from 11º on the closest area to the camera point at the hotel, to 5º at the farthest (Andrade and Ferreira, 2011). Thus, each pixel had different ground coverage/resolution, depending on the corresponding distance to the camera location (hotel). Rectification process was applied to georeference the images, onto the local coordinate system (European Terrestrial Reference System 1989 – ETRS89).

2.4.1.1 OTP GCP sampling strategy

During one of the largest spring tides, at the low tide (~0.2 m HZ), a set of GCPs was collected using a Real Time Kinematic-Global Positioning System (RTK-GPS), Leica Viva GNSS, CS15/GS15 (Leica Geosystems AG, 2012) . This system offers an accuracy better than ± 4 cm and the coordinates were collected in the ETRS89. Hence, some authors referred to it as an accurate method for intertidal field surveys (Hladik and Alber, 2012; Montané and Torres, 2006).
Each collected GCP was coupled with an image (reference images) taken from the fixed

location at the hotel, always keeping the same framework of the entire meadow extension. GCPs collection was carried out as recommended by Finkbeiner et al., 2001: easily visible on the images and distributed homogeneously throughout the target area.

2.4.1.2 OTP georectification process

Georectification was carried out in 2 steps. First, a linear adjustment was applied to all selected OTP images, in order to overlap them to the reference set, taken during the GCPs field survey. Linear adjustment of an image occurs through a 1st order polynomial transformation (Enslin, 2011), which (1) can be written as:

$$p(x, y)=a_1+a_2x+a_3y \quad (1)$$

Where *a* is a computational coefficient derived from the image coordinates *x* (column) and *y* (row) for each selected point (pixel).
This transformation, allows shifting, scaling and rotation of the raster dataset, by entering the coordinates (column, line) for each selected pixel to match from the target image to the coordinate reference (Neteler and Mitasova, 2008). To do so, 15 points from one of the reference images were selected – permanent and fixed buildings present in all images to overlap (e.g Fig. 7).
Even with the OTP images sampling strategy, some small variations in the camera position can occur. Fractions of degree variations in the camera position, can be unnoticed at the first meters foregrounds, but may translate into large variations on the farthest points. Therefore, this first transformation step was applied to correct those errors and to establish similar georectification effects to the complete set of images.

Next, images were rectified, applying a 2nd order polynomial transformation (Enslin, 2011) according to equation (2):

$$p(x, y)=a_1+a_2x+a_3y+a_4x^2+a_5xy+a_6y^2 \quad (2)$$

Fig. 7 OTP2 image overlapped to the reference (OTP5) using 15 pixels as references (red points with yellow/black circles).

This process, besides the linear transformation capabilities, allows bending/distortion of the image. Each GCP point coordinate from the field was match to the corresponding image coordinate (column, row). This relation was carried out visually, checking at pixel level the RTK-GPS system position in the image for each read coordinate taken during the sampling (e.g. Fig. 8). The process was computed for the 3 RGB bands with a nearest neighbor resampling algorithm, in order to obtain a final true-color georectified image derived from the original. All images were rectified together using one of them as the reference for the GCP-pixel matching process. This rectification process, yield truly georeferenced images since all images coordinates were transformed into the local ETRS89 coordinate system as used by the RTK-GPS (Mohammed and Eisa Eiman, 2013).

An exhaustive test was carried on, to perform an optimal GCPs selection over the target, considering the following recommendations (Finkbeiner et al., 2001; Neteler and Mitasova, 2008):

- Homogeneously distributed over the target avoiding lonely GCPs, even if the whole target will not be later used for classification purposes.

- Consider farthest points from the shooting point to be more susceptible to distortions.
- At least double the minimum of GCPs required for the transformation – 2nd degree, 6 GCPs.
- Check both individual and overall RMS errors to avoid large images distortion.

A total of 28 GCP points were used for the 2nd order polynomial georectification of OTP images (e.g. Fig. 8). After the transformation, pixels of the new georeferenced images, had a constant ground resolution, that was set to 0.5×0.5 m, and RGB values derived from the original ones (Andrade and Ferreira, 2011).

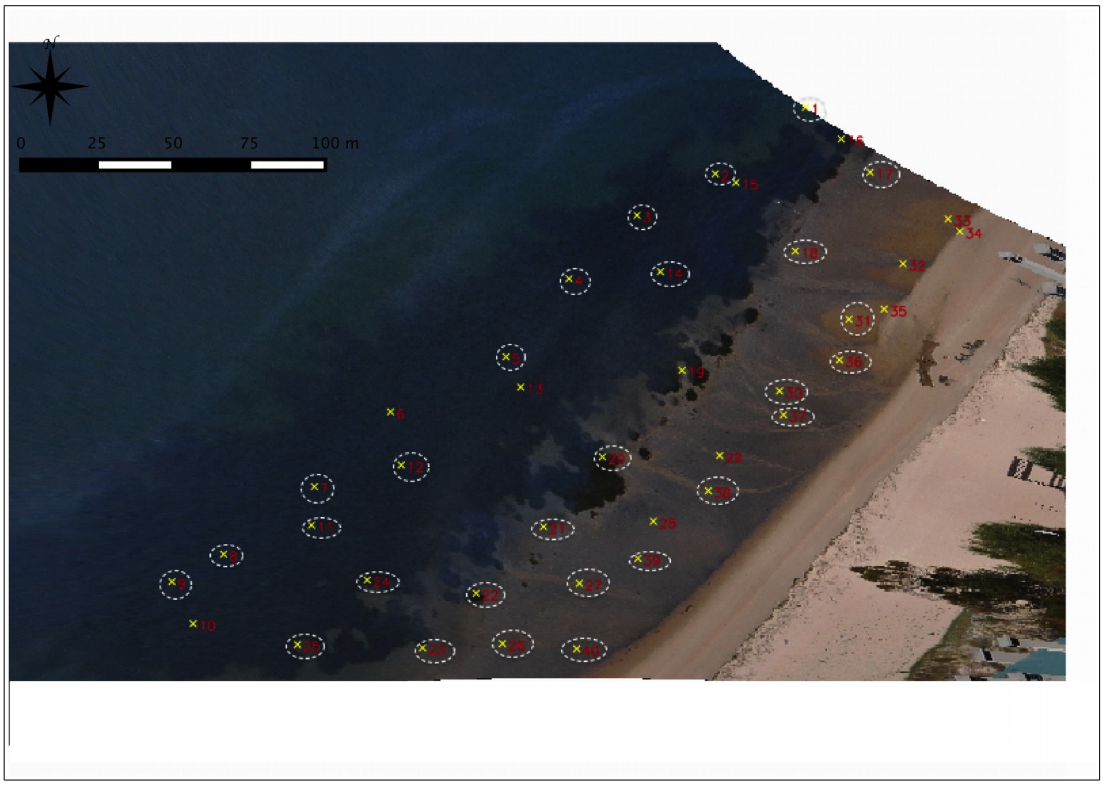

Fig. 8 OTP3 image georectified. White circles highlight the final 28 selected GCP from the total of 40

2.4.2 NAP images

Images obtained from the balloon platform offered a more vertical view than OTP images. Nevertheless the georectification process allowed to correct some camera swing movements.

2.4.2.1 NAP GCP sampling strategy

This approach didn't allowed for the same GCP sampling strategy as OTP images, since it was not possible to determine a relation between automated aerial images and specific ground reference. Ground coordinates data, was therefore registered by surveying the meadow limits with the RTK-GPS system, set to record a coordinate point every 0.5 m (linear distance) with a maximum allowed 2D (x, y) registration error of 0.02 m. The result was a map of 3930 coordinated points (ETRS89) mapping the inshore limit of the meadow, including single small patches (Fig. 9, *a1* and *a2*). This process, was developed during low tide period (~0.4 m HZ) of a spring tide.

This method had 3 main problems: 1) water column visibility; 2) operator accuracy following the edge and detecting patches and 3) to be done temporally close to the balloon images acquisition for a better matching agreement of both.

2.4.2.2 NAP georectification process

By visual observation, some RTK-GPS coordinates (points) where match to the corresponding image coordinates (pixels). This procedure was performed using from both RTK-GPS map and image, some easily and common recognizable shapes to match coordinated points to image pixels.

Differently from the OTP images which all corresponded to the same view of exactly the same ground area, individual NAP images covered different portions of the meadow (Fig. 9, *b*). Therefore, each NAP images had different GCPs combinations. Consequently, each image had to be rectified individually.

Likewise, the rectification process was done running a 2^{nd} order polynomial transformation, with a nearest neighbor resampling algorithm for the 3 RGB bands of each image.

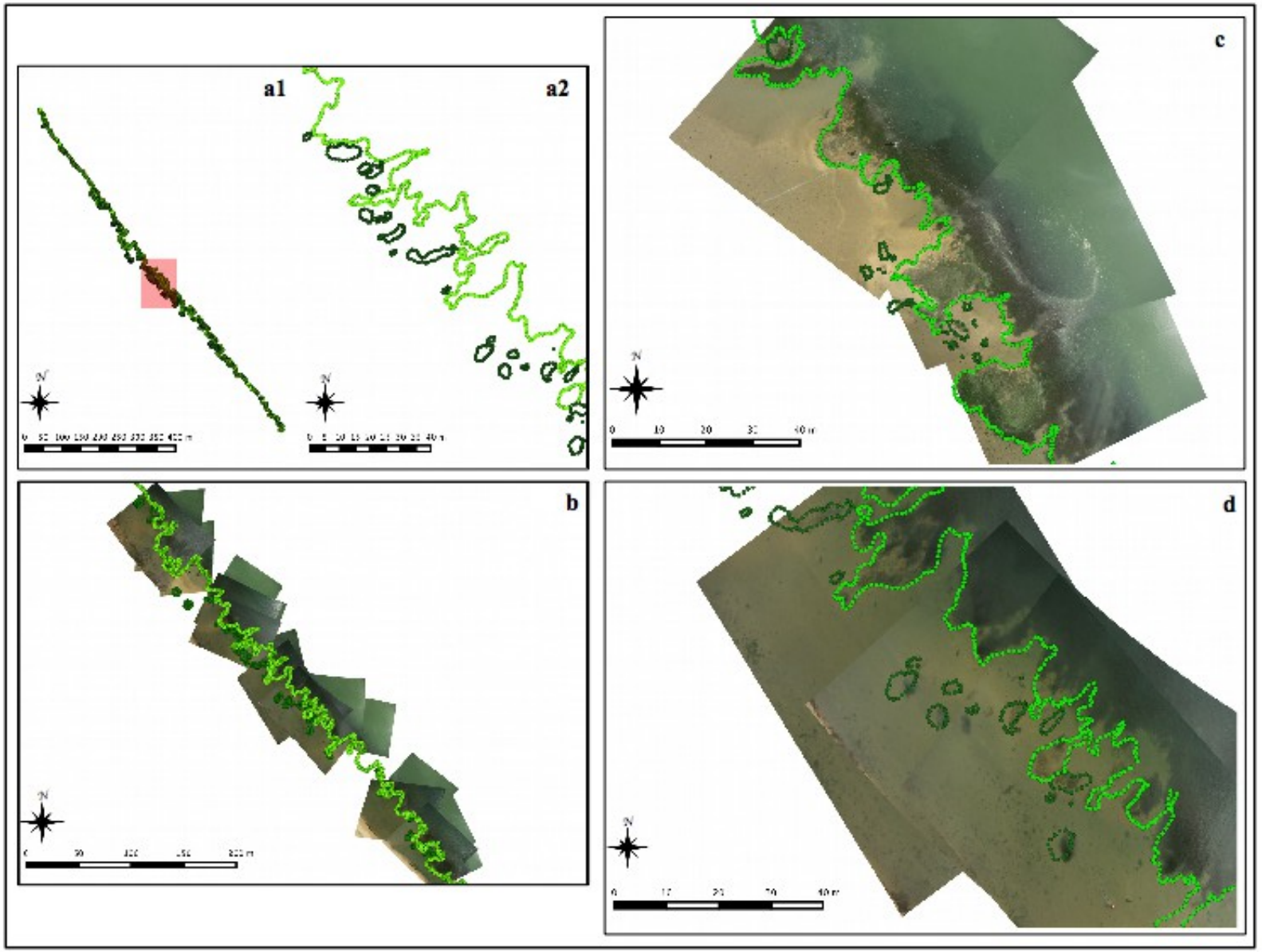

Fig. 9 RTK-GPS points map (a1) with a detailed section (a2) for NAP methodology. All georectified NAP images (b), a southern section of the meadow in emerged sampling conditions (c) and a northern section in submerged sampling conditions (d). Clear green points represents the meadow and dark green points, single patches.

NAP images were georectified with a final resolution set to 0.1×0.1 m. Although the quality of the original images allowed for higher resolutions, it was kept to 0.1 m, since that value allowed for a quantitative and comparative analysis with the 0.5 m resolution of the OTP images, without involving a heavy processing drawback.

Selection of GCPs was more limited than for the OTP images process, considering the need to detect shape similitudes between the RTK-GPS map and each image, to match points and pixels. Nevertheless, the requirement of 6 points per image for the 2nd degree georectification (Enslin, 2011) was always attained, with a minimum of 8 GCPs. Some of the images, however, still did not achieve a minimum desirable quality, mainly due to obliquity induced by the camera balance (Fig. 10). At certain levels of obliquity, NAP images did not allow for a good enough correction even with the rectification transformation, due to the lineal GCP distribution and, furthermore, their limited selection availability.

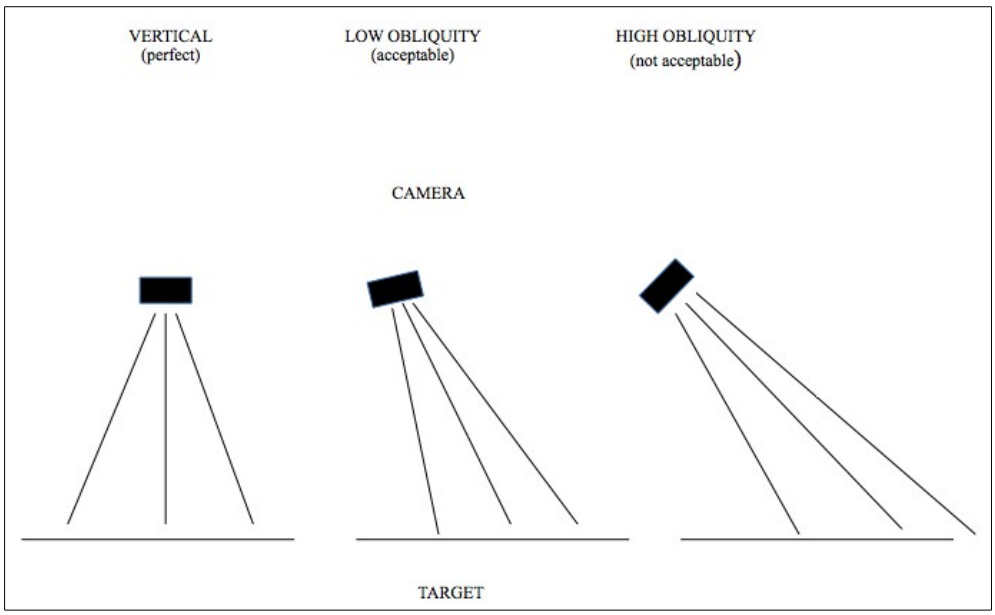

Fig. 10 Camera position and usability of the corresponding images for the NAP approach.

Considering all the above, NAP images were selected considering best quality and combination for the following mosaicking process and representing both emerged and submerged conditions (Fig. 9, *c* and *d*).

For these 18 georectified NAP images, the number of GCPs used per image varied from a minimum of 8 to a maximum of 15, with an average for all images of 11.

2.4.2.3 NAP mosaicking

A stitching process was carried on the georeferenced images to create mosaics representing larger meadow sections. The 10s time-lapse set for the automated shooting mode, allowed an overlapping of ~60% recommended for the mosaicking (Bendell and Wan, 2011; Grenzdörffer et al., 2008).

The 18 georectified NAP images were stitched in groups of 2 or 3, creating a total of 8 mosaics for different meadow sections – 4 for emerged and 4 for submerged conditions by pairs as represented in Table 2.
Although image stitching was done based on their actual coordinates (taken from the RTK-GPS survey), some previous tests on their optimal overlapping position were carried out to decide on best visual results.
Using the RTK-GPS map as a visual ground reference, stitching process was performed selecting best contiguous images to match, in order to minimize seams visual effects (e.g. Fig. 11) (Muise, 2010).
Color balancing can be used to equalize differences between stitched images in a mosaic. However, as noticed by Turner et al., 2012 that could lead to final quantifications bias due to changes in the visual integrity of each individual image.

2.5 Masking

After the georegistration process a total of 16 georectified true-color images was obtained for the two methodologies: OTP (8 images representing emerged and submerged conditions by pairs) and NAP (8 mosaics of images representing emerged and submerged conditions by pairs).

Those images, however, did not offered same quality across all the represented meadow, either because georectification distortions or because sampling conditions.
OTP images had the worst meadow visibility at the deepest edge (offshore), mainly due to the water depth. Moreover, because of the distance from the observation point, this meadow limit had higher GCPs individual RMS error and, consequently, greater distortions (Fig. 8). Hence, a mask was applied to those set of images, retaining only a window of the target meadow area, avoiding at the same time irrelevant features (Andrade and Ferreira, 2011). Masks were set up from vectorial polygons manually created over the desired portion of the image.

Depending on conditions, each selected image showed different usable portions of the meadow. Considering the objective of comparing emerged and submerged conditions, the most limiting common area with good meadow visibility was delimited which corresponded to the mask delimitation.

NAP mosaics on the other hand, did not have as higher rectification distortions as OTP images, nevertheless, a mask was applied to each mosaic created (e.g. Fig. 11), to discard the worst meadow visibility edge (offshore) and, likewise, to avoid irrelevant features and to enhance processing time (Macleod and Congalton, 1998).

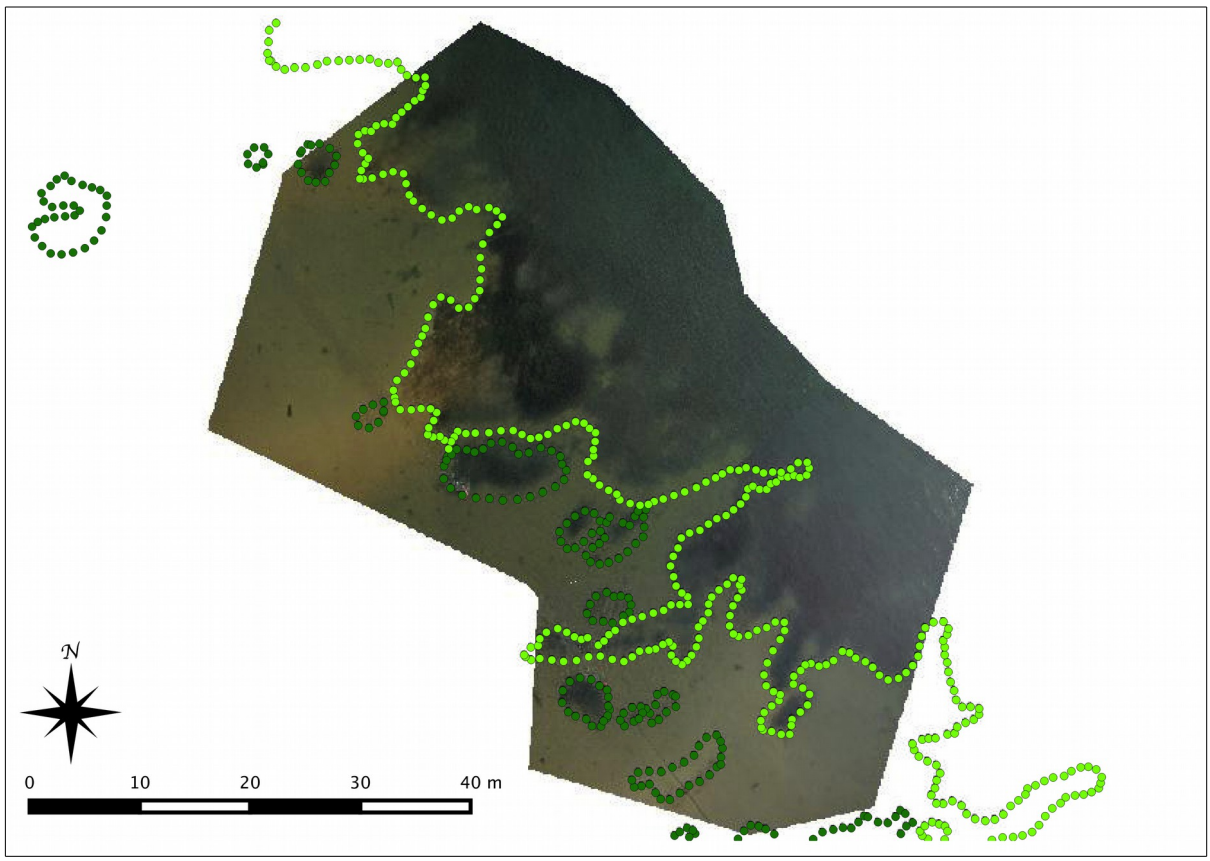

Fig. 11 Mosaic from 2 georectified pictures using the RTK-GPS surveyed meadow (clear green points) and patches limits (dark green), to create NAP4 image representing a submerged condition and masked for undesired features.

2.6 Images classification

Masked georectified images and mosaics (OTP and NAP), were next classified. Images classification process was done using true color information for their 3 spectral bands – red

(R: λ 0.6 – 0.7 μm), green (G: λ 0.5 – 0.6 μm) and blue (B: λ 0.4 – 0.5 μm) (Jensen, 2005; Neteler and Mitasova, 2008). Each pixel from each image taken have a specific value that represents a spectral signature captured from the photographed target. Thus, spectral signatures registered by the photograph, being captured as numerical values, can be selected (classified) for image analysis purposes.
Classification of these habitats based on their true-color spectral signatures, has been shown to be an accurate methodology at different scales and resolutions (Andrade and Ferreira, 2011; Hashim et al., 2014). Furthermore, visual comparison of classification results with the original true-color compositions helped on classification decisions.

Using GRASS GIS, two classification techniques were used to test different approaches on the optimization of image processing and analysis for the present research (Fig. 2 and 3): pixel-based classification and object-based classification. Both were applied to all 8 OTP images and 8 NAP mosaics.

2.6.1 Pixel-based classification

This classification technique is a radiometric classification where first, the data is analyzed for spectral signatures similarities and then, pixels are assigned to classes based on their similarity (Neteler and Mitasova, 2008). Pixel-based classification can be implemented either through a supervised or an unsupervised process.

In the supervised classification, “training areas” are defined by the analyst, based upon his/her terrain knowledge, for statistical assessment of class spectral signatures that are then extrapolated to the entire image. Unsupervised classification automatically assigns pixels to spectral classes (Neteler and Mitasova, 2008). Some authors have referred to the advantages of supervised approaches over unsupervised when separating spectral signatures (Nayak and Behera, 2009; Thomson, 1998), since the process is more reliant to user control. However, as other authors noticed (Banman, 2002; Jensen, 2005), analyst experience and subjectivity, are concerns to consider. Hence, some studies highlighted better accuracy results under unsupervised classifications than supervised, due to those human induced errors (Banman, 2002; Jensen, 2005) .
Moreover, the research conducted by Andrade and Ferreira, 2011 at the same study site as the present research, with common methodology procedures, showed a high classification

accuracy (average of 94%) with an unsupervised classification methodology. Thereby, and with the goal to test and compare pixel-based classification between approaches, the present study was performed with an unsupervised classification. This image processing included 2 steps in GRASS GIS: 1) preprocessing (clustering) and 2) classification.

2.6.1.1 Preprocessing – clustering

Using a clustering algorithm, spectral signatures representing land cover types are generated in each image (Shapiro, 2012a). This algorithm creates pixel clusters based on the spectral signatures from the pixels of the raster.
For the computational process, the number of iterations was set to a maximum of 30 and maximum number of classes created (clusters) to 50 (Dogan et al., 2009; Thomson, 1998). Whenever number of clusters reached the maximum designed by the analyst, the process was repeated increasing the number of iterations (Shapiro, 2012a). It is remarkable that, while OTP images didn't need this iterations increase at all, NAP images needed it more than once. This was expectable given the higher resolution and corresponding heterogeneity of NAP images.

2.6.1.2 Classification

Using the Maximum Likelihood Classifier (MLC), the software classifies the spectral signatures information created by the clustering algorithm. The MLC use this information to determine to which category each cell in the image has the highest probability of belonging (Shapiro, 2012b). Thus, the true-color raster is transformed to a 50 classes raster (e.g. Fig. 12, *a*).

2.6.2 Object-based classification

While some discrepancies are found in the literature when comparing unsupervised and supervised pixel-based classification, there seems to be a greater consensus on the better classification accuracies from object-based approaches over pixel-based, not only for coastal habitats but also for many land cover classifications (Dupuy et al., 2012; Hölbling et al., 2012; Huth et al., 2012; Kamal and Phinn, 2011; Vo et al., 2013; Wang et al., 2004; Yan et al., 2006).

Differently from pixel-based classifications, the grouping criteria in this approach not only responds to the spectral signature of pixels, but to their contiguity as well. Pixels, are recognized as individual objects that can be grouped with contiguous pixels with similar spectral signatures (Benz et al., 2004). Thus, a new group of pixels is a larger object called a segment. Each generated segment, now has a new identity (value) making it more or less susceptible to be merged with neighboring segments, into a new larger object (Aplin and Smith, 2011). This process can be repeated as many times as required by the analyst, with different sensibilities depending on the input parameters. Our strategy, was to perform a hierarchical segmentation (Hölbling et al., 2012; Urbański et al., 2009).

When computing the segmentation on GRASS GIS, the user may decide on the threshold of this process. Threshold values, rang from 0.0 to 1.0. Lowest values computes a merging of only objects with the exact same identity (spectral signature) while the largest value allows for merging of all objects (Momsen and Metz, 2015). Hierarchical segmentation starts with low threshold values, which produces a new highly segmented raster. This new raster is then used as a seed for a next computing segmentation process with a higher threshold value, the process being repeated as many times as the analyst defines (e.g. Fig. 13 *a* and *b*). First segmentation threshold was set to 0.01 threshold, then to 0.02, 0.03 and so on. Iterations were set to a maximum of 20, in all cases this value was reached. The process is executed using a region-growing-merging algorithm (Momsen and Metz, 2015).

Hierarchical segmentation generates groups of larger objects at each step, by generalizing the spectral signature between neighboring objects. Although this promotes an improvement in the efficiency of classification, this feature has the risk of merging objects from different classes into a single one (new larger object). This handicap becomes more evident along different classes edges (Wang et al., 2004). Additionally, this effect worsens when characterizing some marine habitats, where frontiers between categories are often fuzzy (Lucieer, 2008). As noticed by Roelfsema et al., 2014, this classification approach to seagrass meadows can be sometimes tricky due to the water column optical properties. Indeed, at some point of the hierarchical segmentation, the next step will tend to incorporate isolated small seagrass patches into a no-seagrass class which may happen at different scales namely due to the water column visibility. To avoid such wrong interpretations, hierarchical segmentation was performed onto each image until some small patch or boundary was wrongly classified by the algorithm, which usually happened for small fuzzy attributes of the image. Then, the immediate previous step was selected.

2.7 Reclassification

Classifications methods, produced rasters of pixels (pixel-based algorithm) or objects (object-based algorithm) representing the target areas. These rasters had to be reclassified using the analyst visual rules, grouping all occurring categories until a binary image was obtained for seagrass and non-seagrass areas (e.g. Fig. 12, *b* and Fig. 13, *c*).

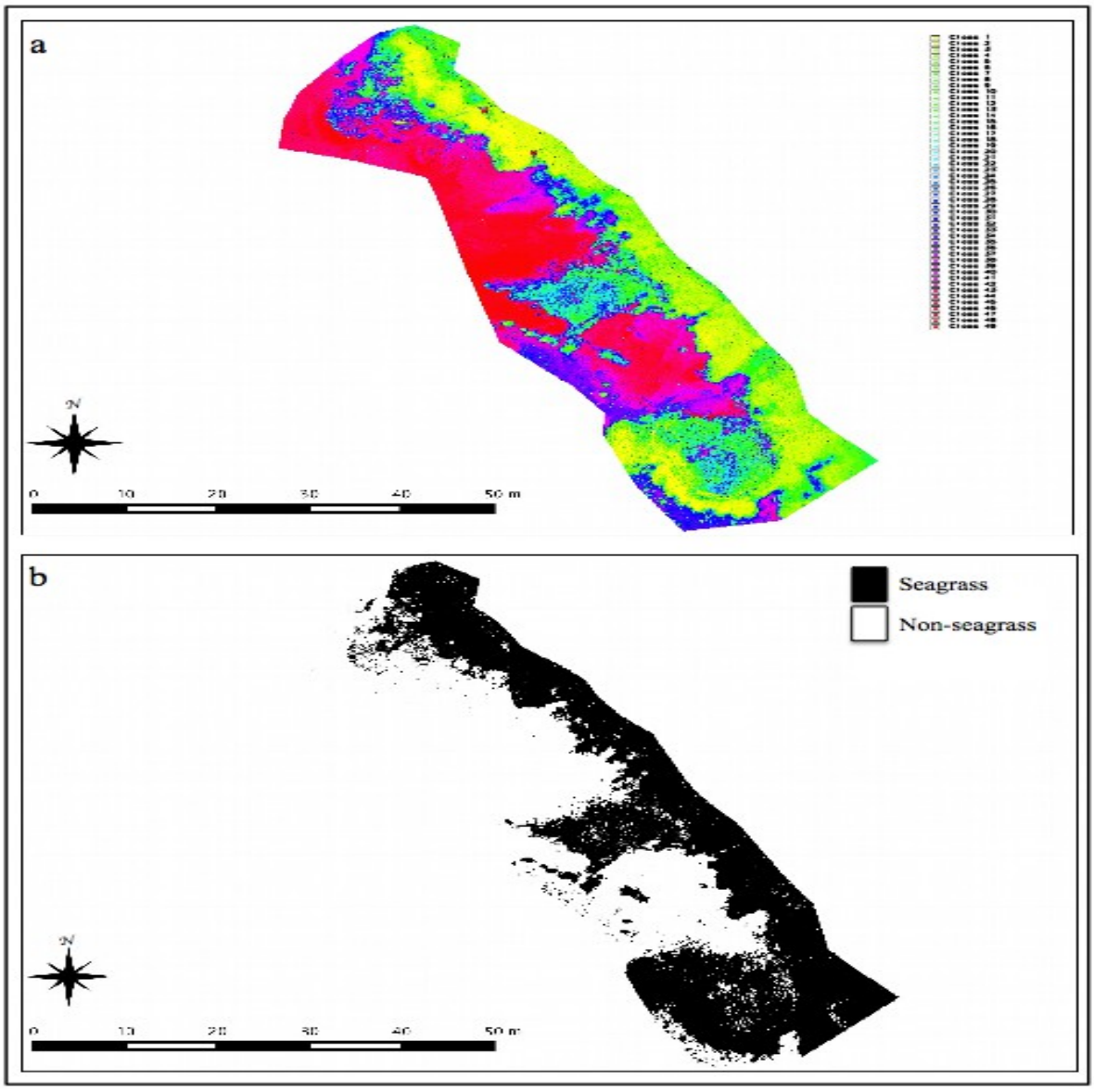

Fig. 12 First 50 clustering classes (a) and final reclassified binary map (b) with seagrass and no seagrass classes for NAP7 image.

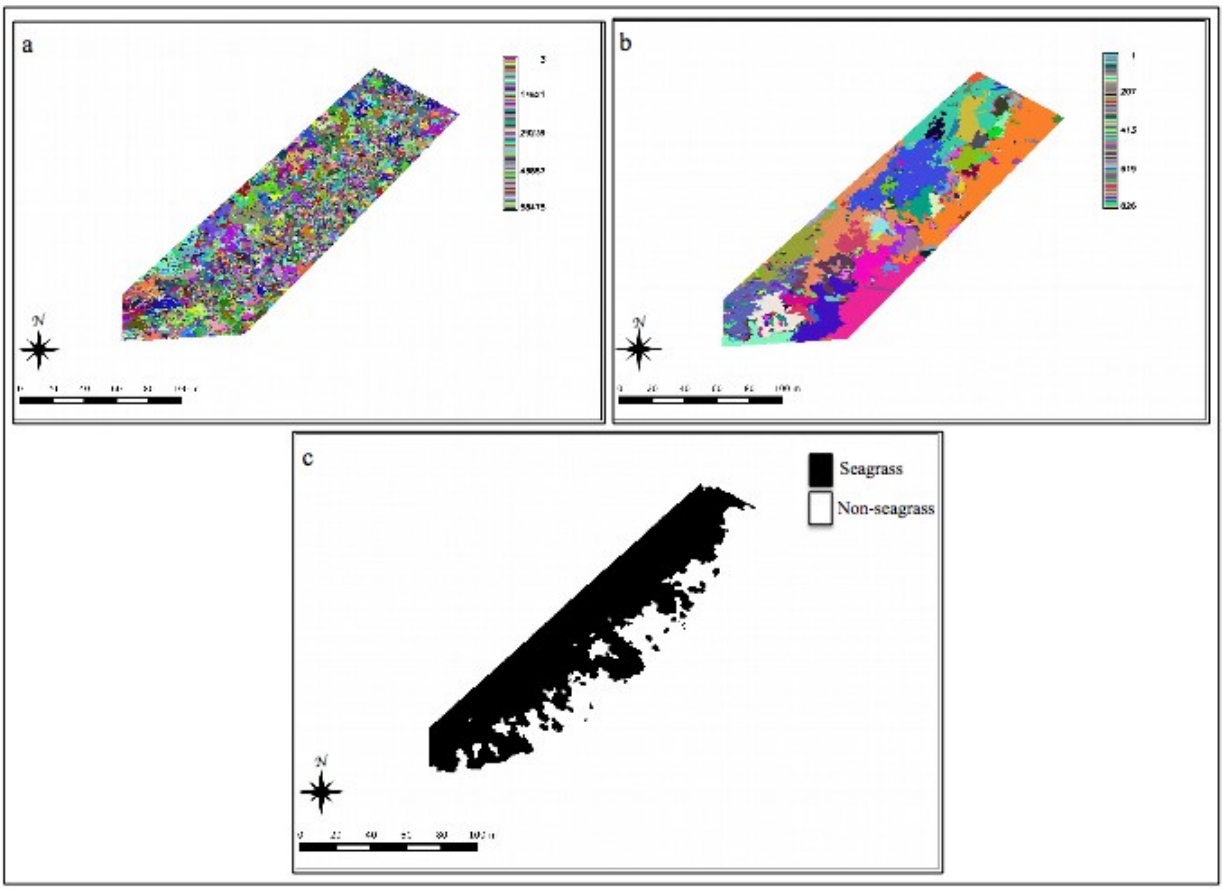

Fig. 13 Object-based classification of georectified and masked OTP2 image, using hierarchical segmentation process. Represented on the first stages of segmentation (a) with a high segmented raster map, a middle hierarchical segmentation stage with a larger objects (b) and final binary map after the reclassification of the objects (c).

Although (Andrade and Ferreira, 2011) suggested a mode filter to clean this final binary result, we decided to avoid this step since cleaning of results could affect comparison of the accuracy classification methodologies.

2.8 Data from processed images

After all image processing steps were concluded (Fig. 2 and 3), 32 binary rasters were obtained, 16 for each methodology (OTP, NAP): 4 pairs for each methodology representing both conditions per couple (1-emerged, 2-submerged; 3-emerged, 4-submerged;…) and each image classified with both approaches (pixel-based, object-based).
Fig. 14 illustrates an example with 2 pairs of images from each methodology (OTP/NAP) representing each condition (emerged/submerged) through both classifications applied (pixel-based/object-based).

From final binary rasters, two data information were extracted: area and classification accuracy. Additionally a kappa coefficient analysis (Cohen, 1960) was realized comparing binary rasters (Wen, 2014).

2.8.1 Area variations

The interest of area variations relapsed at sampling condition level comparison. Considering that each pair of images, representing emerged and submerged condition of the same exact location and framework, were taken temporally close, possible changes in the meadow due to natural seagrass growth were not considered. Then, for each methodology separately, all meadow areas from emerged conditions were compared to all meadow areas from submerged conditions, using both pixel-based and object -based classifications mapping data.

2.8.2 Classification accuracy

Accuracy assessment is the comparison of the classified image to the reality/real world. This comparison can be made at pixel or group of pixels level. Often, this test is made through field samplings, recording several coordinates of the presence/absence of each class present in the final classified map (Jensen, 2005), but there is not a standardized practice agreed on by all researchers (Foody, 2002).

Seagrass meadows, as other marine habitats, are not static systems. Even more, constant hydrodynamic and weather phenomena, as well as eventual anthropogenic effects during the observation period, clearly determine the features of the image taken and its analysis. In this context, sampling in-situ ground truth points, should be done at the same time of each image taken to ensure the image-field correspondence. This is certainly not achievable when shooting an image every 2 minutes (OTP), or every 10 seconds from a moving platform (NAP). Furthermore, *in-situ* sampling for accuracy assessment can be considered a contradiction when the purpose is the remote sensing classification. Assessing the accuracy through selected points on the original

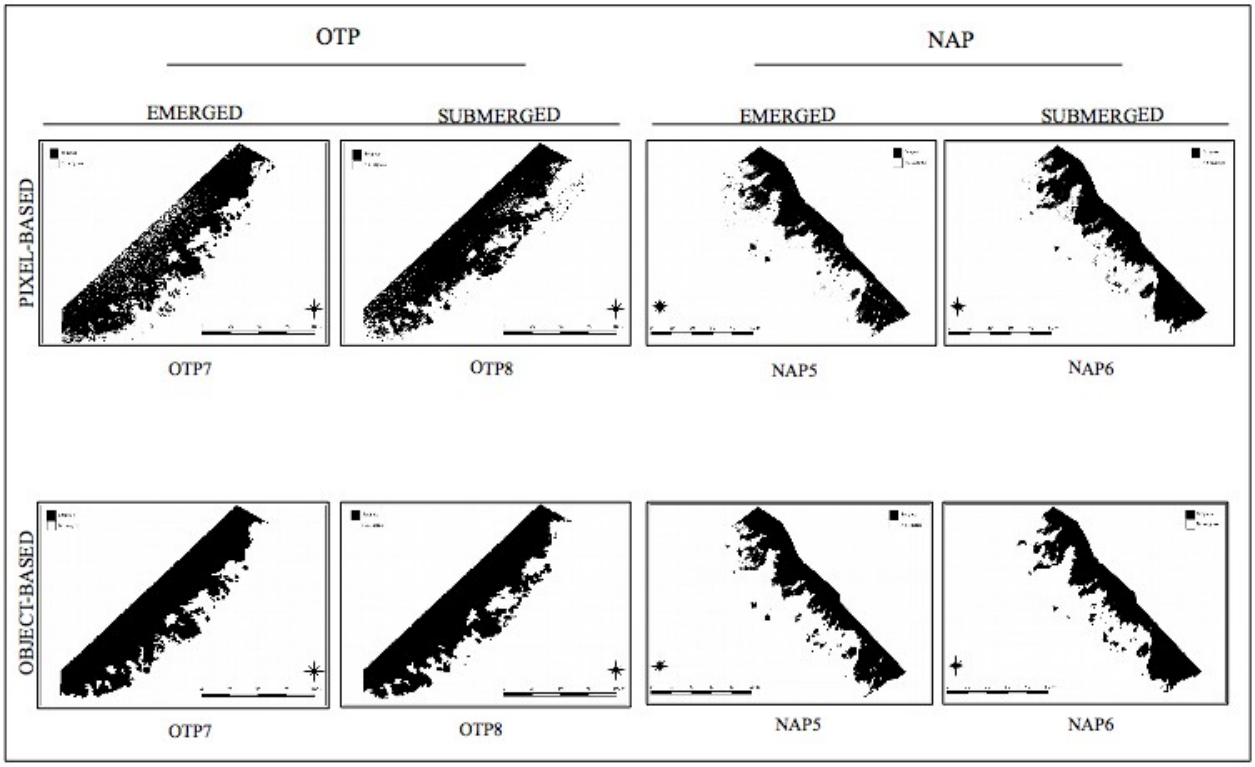

Fig. 14 Pair of images (OTP7 and OTP8; NAP5 and NAP6) for each methodology (OTP and NAP), obtained at both conditions emerged and submerged (temporally close and at the same exact location with same framework) and, each, classified with pixel-based and object-based classification.

image, by visual interpretation, can be a wise decision in this case (Jensen, 2005; Urbański et al., 2009).

There is not a strict rule for the number of points to use for the accuracy assessment of a classification. Congalton, 1991 concluded that 50 ground truth points would be the minimum to consider for each category and, for large areas (>4×10^5 h) or many categories classified, increase to 75 or 100 points per category. Over the years, Congalton, 1991 considerations, has been widely applied in many researches (Foody, 2008, 2002).

Our study areas were far from those 4×10^5 hectares and only 2 classes were targeted. Nevertheless, to strongly support the methodology, a total of 160 points (80 for Seagrass class and 80 for No Seagrass class) were used to assess accuracy of each of the 32 final classified rasters. Original images used for the definition of ground control points, were the true-color georectified images (OTP) and mosaics (NAP). Points were spread over these true-color images, intentionally including some tricky spots such as low density seagrass or fuzzy patches (e.g. Fig. 15).

Due to the previously commented handicaps, for submerged vegetation, accuracy was assessed allowing for a 9 pixel kernel tolerance around each ground truth point (Dogan et al.,

2009), which covers 8 pixels surrounding the actual position pixel.
Overall accuracy is then calculated using an error matrix (Congalton, 1991; Jensen, 2005).

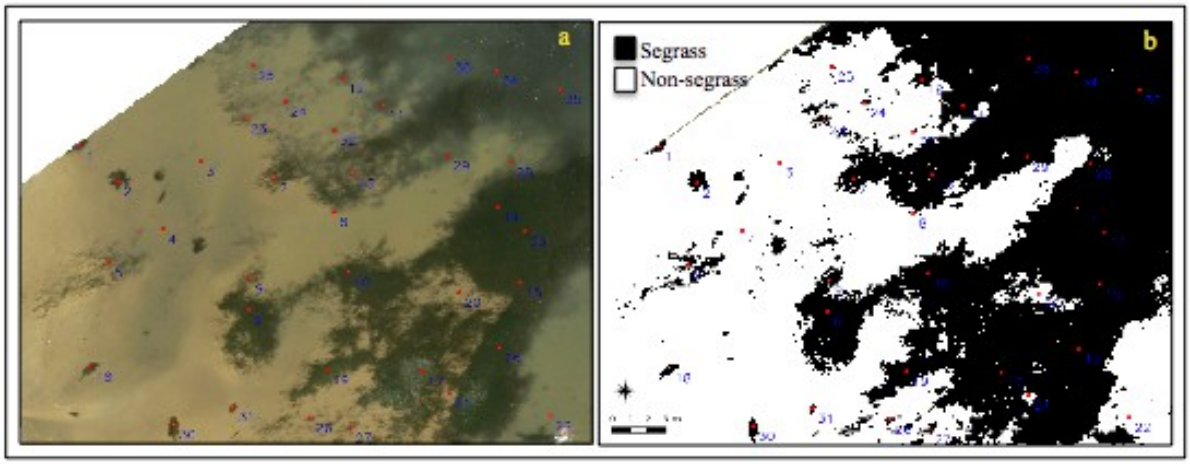

Fig. 15 Detailed section of NAP5 image with ground truth points for accuracy assessment over the true-color image (a) and the pixel-based classified binary image (b).

2.8.3 Kappa analysis

With the aim to test for possible mapping differences between classification approaches, a kappa analysis was carried out. The Kappa coefficient is a statistic analysis that estimates the agreement of classification between two maps (Jensen, 2005). This test was done by comparing one-to-one the 4 classified maps (2 classifications for each condition) obtained from each pair of images.

Kappa values > 0.80 indicates strong agreements between the 2 compared maps, between 0.80 and 0.40, a moderate agreement and < 0.40, a poor agreement (Jensen, 2005).

2.9 Statistical analysis

Statistical analysis was carried out to test for differences/similitudes from data obtained of the processed images (areas, classification accuracies and kappa analysis) in the 3 proposed levels comparisons context, were the null hypothesis (H_0) was accepted for p-values ≥ 0.05 and rejected for p-values < 0.05:

- Areas variations: H_0 – Seagrass meadow areas do not differ between emerged and submerged conditions for any of the two image acquisition methodologies.

- Classification accuracies: H_0 – Classification accuracies do not differ for any level of comparison (methodology, sampling conditions or image classification).
- Kappa analysis: H_0 – binary maps do not differ when compared between pairs of images for sampling conditions or image classification level.

3 RESULTS

Results for Georectification process were obtained from GRASS and QGIS rectifying tools.

Results for areas, image classifications and kappa coefficient were obtained from GRASS and statistically analyzed with free software R Statistics (R Statistics, 2008). Data was first tested for its normality with a Shapiro-Wilk test. Since data did not had normal distribution in any case (Shapiro-Wilk: $p < 0.05$), differences between data, were tested applying a non-parametric Kruskal-Wallis test (Kruskal and Wallis, 1952). This test, calculates the significance of differences (significantly different when $p<0.05$) between means ($\bar{\chi}$) of two or more independent groups with a non-normal distribution of the data. The test is reported in R with the test statistic labeled as chi-square (χ^2), the degrees of freedom (df) and the significance (p-value or *p*) (Field et al., 2012).

3.1 Georectification

The average root mean square error (RMS error) for the 1st polynomial transformation of OTP images, was 0.0372 pixel units. This is, overlapped images had an average pixel error position of 0.0372 pixels from the reference image. For the further 2nd polynomial transformation, the overall RMS error was 1.3885 which corresponds to 0.6690 ground meters.

For the NAP images georectified for the next mosaicking process, the RMS error ranged from a minimum of 0.8626 to a maximum of 1.9741 with an average of 1.3305, corresponding to a 0.1330 ground meters since resolution was set to 0.1 m.

3.2 Area variations

In OTP images, classified areas between pairs varied largely, ranging from areas < 10^3 m^2 to areas > 8×10^3 m^2 (Fig. 16, *a*). However, those variations were between different pairs due to the different mask applied. For the target area resulting from application of the common mask, differences between conditions emerged ($\bar{\chi}$= 4.819×10^3 m^2) and submerged ($\bar{\chi}$= 4.757×10^3 m^2), were not significantly different (χ^2=0.0993; df=1; p=0.7527).

For NAP mosaics, areas did not have such large differences between pairs (Fig. 16, *b*), with values from 9×10^2 to 1.637×10^3 m^2. The comparison between conditions emerged ($\bar{\chi}$= 1.279×10^3 m^2) and submerged ($\bar{\chi}$=1.287×10^3 m^2) did not show significant differences (χ^2=0.0110; df=1; p=0.9164).

3.3 Classification accuracy

Accuracies were calculated throughout matrix errors for each binary map obtained as represented in the example from Table 3. From this matrix 3, accuracies were obtained for each map: producer's accuracy, user's accuracy and overall accuracy. Overall accuracies for each map are the ones used for the statistical analysis, referred to the comparative test between classification accuracies.

Accuracies ranged from 77% to 100% with an overall average of 92%.

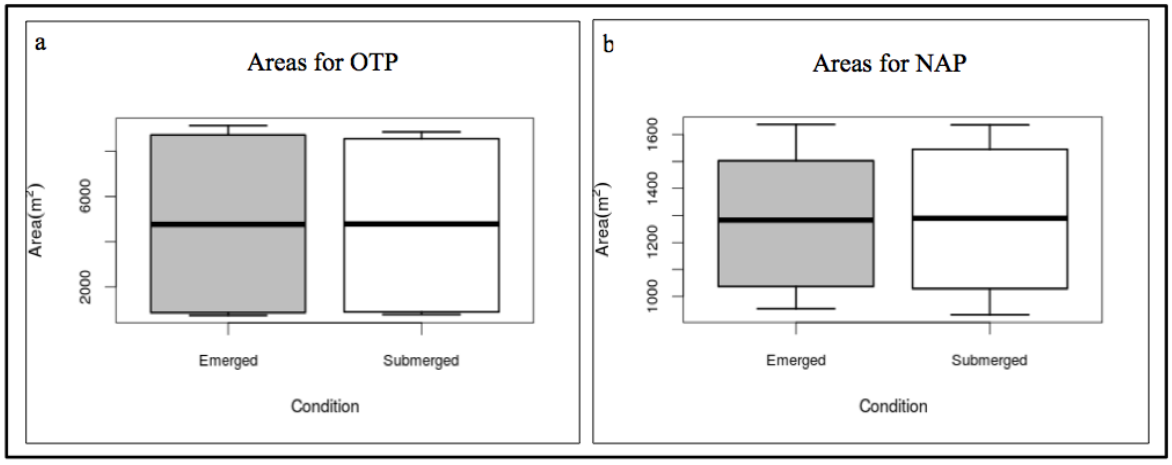

Fig. 16 Area values range for emerged and submerged conditions of OTP (a) and NAP (b) final binary maps *(p>0.05)*

Table 3 Overall accuracy (90%), Producer's accuracy and User's accuracies for pixel-based classification of NAP4 image. Grey shadow highlights correct observations of remote sensing classification for each class (Seagrass and Non-seagrass), tested against reference data.

		Reference data		
	Class	Seagrass	Non-seagrass	Row total
Remote sensing Classification	Seagrass	71	7	78
	Non-seagrass	9	73	82
	Column total	80	80	160

Overall Accuracy=(71+73)/160=90%

Producer's Accuracy (omission error)			
Seagrass	71/80 =	88.75%	11.25% (omission error)
Non-Seagrass	73/80 =	91.25%	8.75% (omission error)
User's Accuracy (commission error)			
Seagrass	71/78 =	91.03%	8.97% (commission error)
Non-Seagrass	73/82 =	89.02%	10.98% (commission error)

Results for methodologies, basically reflect accuracies which depend on the acquisition and georectification features: mainly the final resolution selected and the level of image distortion. OTP accuracies ranged from 83% to the maximum (100%) from the overall values of all OTP images accuracies calculated, with an average of 93% (Fig. 17). NAP methodology values, on the other hand, ranged from a minimum of 77% and the maximum (100%), with an average of 91%. (Fig. 17). Accuracies were not significantly different at methodology level (χ^2=1.5087; df=1; p=0.2193).

For the condition level, accuracies for emerged ranged from 82% to 98% with an average value of 91% (Fig. 18). Submerged class showed a wider range, from a minimum of 77%, to the maximum, 100%, with an average of 93% (Fig. 18). Accuracy did not differ significantly between emerged and submerged conditions in OTP nor NAP (χ^2=1.8; df=1; p=0.1797). Although the differences are very similar, it is noticeable that these occur over the low dense patches referred above.

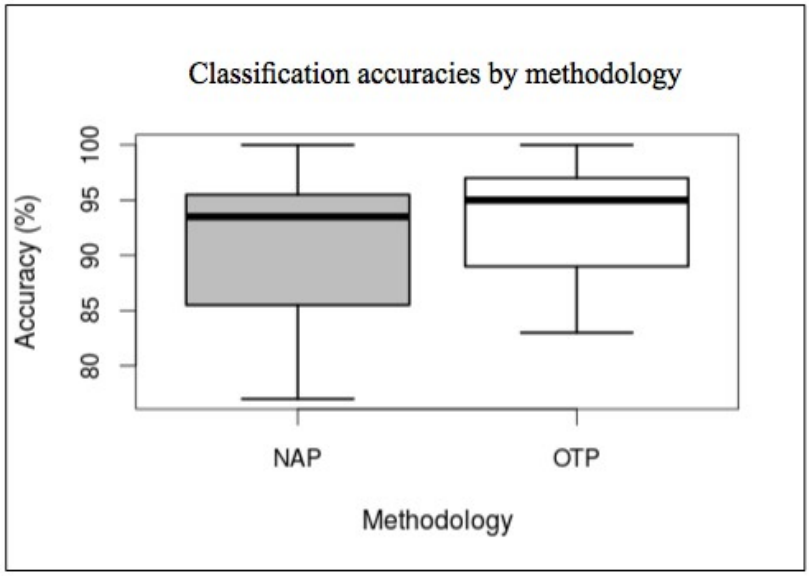

Fig. 17 Classification accuracies range for NAP and OTP (p>0.05).

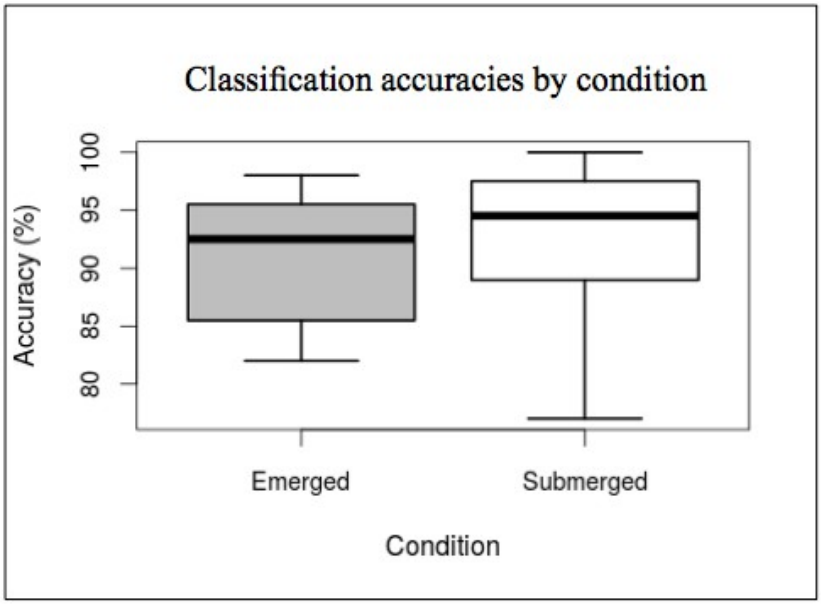

Fig. 18 Classification accuracies range for emerged and classification accuracy (p>0.05).

Comparing classifications accuracy for each image classification approach, values showed the highest differences. Pixel-based classification varied from a minimum value of 77%, to 96%, with an average of 87% (Fig. 19). While object-based approach had a range from 93% to the

maximum value of 100%, with an average of 96% (Fig. 19). Accuracies were significantly different between pixel-based and object-based classifications (χ^2=17.283; df=1; p=3.221×10^{-05}). Object-based accuracy results were higher for both OTP and NAP methodologies (96% each) compared to pixel-based accuracy (86 and 90% respectively).

For both comparison levels, condition and classification, NAP images showed remarkable differences over patches or fractions of the meadow with low density (e.g. Fig. 15). Also in NAP image sets, the eventual presence of other intertidal marine vegetation (e.g. *Ulva* spp.), lead to higher classification problems with pixel-based classification than with object-based. On OTP images, for pixel-based classification, the incorrect classification of meadow presence, occurs most commonly over dark areas (e.g. stirred sand by some fisherman). The object-based approach overcame those issues, with patches with small and low density individuals yielding the most common inaccurate results.

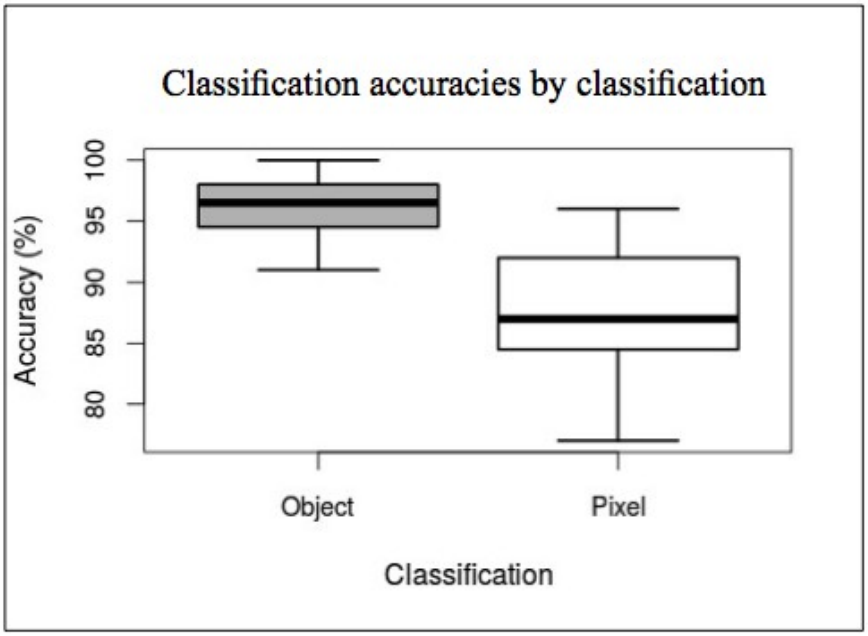

Fig. 19 Classification accuracies range for object-based (Object) and pixel-based (Pixel) classifications (p<0.05).

3.4 Kappa analysis

The kappa analysis produced a matrix with the 4 binary maps of each pair of images comparing emerged/submerged conditions (e/s) and pixel-based/object-based (p/o)

classifications. Their respective cross-linked combinations are presented in the example on Table 4.

Table 4 Kappa values (lower left) and variation (upper right) resulting from the comparison of OTP1 (Emerged) and OTP2 (Submerged) with both pixel-based and object-based classifications, through kappa analysis between binary maps.

Classification		Pixel-based		Object-based	
	Condition	Emerged	Submerged	Emerged	Submerged
Pixel-based	Emerged		$4x10^{-6}$	$3X10^{-6}$	$4x10^{-6}$
	Submerged	0.8895		$2x10^{-6}$	$2x10^{-6}$
Object-based	Emerged	0.9041	0.9281		$2x10^{-6}$
	Submerged	0.8932	0.9388	0.9471	

Each resulted cross-linked combination for OTP and NAP pair resulted from the cross-link comparisons, as instantiated in Table 4, are represented in Tables 5 and 6 respectively.

For the OTP methodology, average values for each binary maps pair comparison by kappa analysis, ranged from 0.6485 to 0.8771, with an overall average for all OTP comparisons of 0.7544 and a variance $\leq 8.2\times10^{-4}$ (Table 5). Kappa analysis results were not significantly different for any comparison pair within OTP methodology (χ^2=7.32; df=5; p=0.1979).

For NAP methodology, average values for each binary maps pair comparison by kappa analysis, ranged from 0.6149 to 0.7895, with an overall average for all NAP comparisons of 0.7002 and a variance $\leq 4\times10^{-6}$(Table 6). Kappa analysis results were not significantly different for any comparison pair within NAP methodology (χ^2=5.33; df=5; p=0.3769).

Higher kappa levels were found, for any methodology, when comparing maps corresponding to similar conditions (emerged or submerged). Lowest values were found when comparing different conditions and different classification methods combined, as well as between different conditions for pixel-based classifications (Fig. 20).

Table 5 Kappa values for each images pair of OTP, comparing final binary rasters obtained from emerged (e) or submerged (s) condition with object-based (o) or pixel-based classification (p).

		Classifications and conditions comparisons					
		oe – os	ps – os	pe – os	ps – oe	pe – oe	pe – ps
Images pairs	OTP1/OTP2	0.9471	0.9388	0.8932	0.9281	0.9041	0.8895
	OTP3/OTP4	0.7150	0.8177	0.7178	0.6370	0.9453	0.6356
	OTP5/OTP6	0.5154	0.8937	0.5157	0.4840	0.8310	0.4827
	OTP7/OTP8	0.7983	0.8584	0.6482	0.7288	0.7945	0.5862
	Average	0.7440	0.8771	0.6937	0.6944	0.8687	0.6485
Overall Average =		0.7544					
Average variance ≤		$82x10^{-5}$					

Table 6 Kappa values for each images pair of NAP, comparing final binary rasters obtained from emerged (e) or submerged (s) condition with object-based (o) or pixel-based classification (p).

		Classifications and conditions comparisons					
		oe – os	ps – os	pe – os	ps – oe	pe – oe	pe – ps
Images pairs	NAP1/NAP2	0.5791	0.5935	0.4787	0.4636	0.7008	0.4512
	NAP3/NAP4	0.8352	0.8381	0.7885	0.7689	0.8173	0.7676
	NAP5/NAP6	0.7466	0.8594	0.7400	0.7443	0.8409	0.7509
	NAP7/NAP8	0.5991	0.7432	0.5608	0.6692	0.7989	0.6695
	Average	0.6900	0.7586	0.6420	0.6615	0.7895	0.6598
Overall Average =		0.7002					
Average variance ≤		4×10^{-6}					

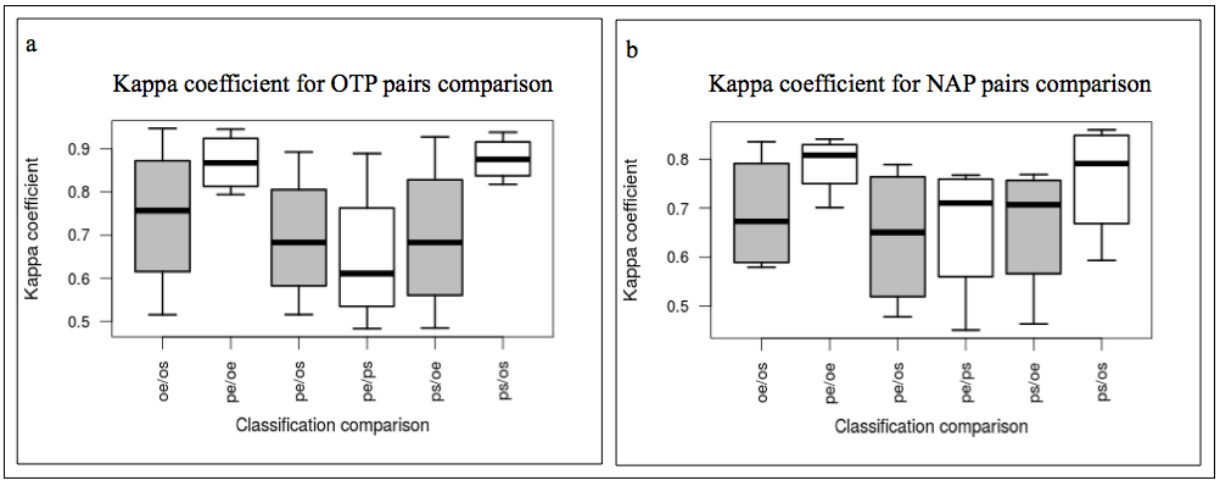

Fig 20 Kappa coefficient values range for OTP (a) and NAP (b) images, comparing final binary rasters obtained from object-based (o) or pixel-based classification (p) and emerged (e) or submerged (s) condition (p>0.05).

4 DISCUSSION

Despite Andrade and Ferreira, 2011 methodology offering great advantages over other approaches, as the authors concluded, some issues conditioned the image acquisition and its further processing and interpretation. Our new methodology was tested against the one proposed by these authors, in order to overcome or optimize some of the limitations cited. The test was done through the images taken and processed, to analyze three levels of the proposed approach: Image acquisition (methodology), sampling conditions and image classification.

Image acquisition (methodology)

While tide level (> 0.8 m HZ) and water transparency similarly affect both methodologies, wind is undoubtedly a greater limitation for NAP methodology. Still, our proposed prototype of balloon system (Fig. 6) offers stability during the sampling process even with eventual wind rafts of up to 6 knots.

Either way, NAP methodology offers several additional advantages. First of all, the balloon system can be deployed at any location without the need of an elevated point from where to take images. Furthermore, NAP methodology allows for images to be taken at lower distances from the target which, combined with a higher resolution, offers images with more detail than OTP, clearly an advantage for ecological studies (Banks and Skilleter, 2007; Boyle et al., 2014).

Also, the altitude (50 m) combined with the almost nadir view, allowed for framing of the complete width of the meadow with much lower distortions on the georeferencing process (overall RMS ~0.1330 ground meters) when compared to the oblique images acquired from the hotel in the OTP (overall RMS ~0.6690 ground meters). Finally, the CHDK settings, allowed for an adequate amount of images being taken, as recommended by (Lonneville et al., 2013) for the overlapping process. Yet, the stitching process needed for the NAP methodology, may be an extra issue to consider for the final images quality (Koh and Wich, 2012).

When comparing classification accuracies for methodology level (Fig. 17), higher resolution images obtained from the balloon did not offer better results (p=0.2193), which can be argued for some reasons: Typical leaves length ranges from 0.2 to 0.8 m for the two seagrass species occurring at the study location – *Zostera marina* and *Zostera noltii* (Moore and Short, 2006). Thus, considering that pixel resolution puts the limit of change detection in digital imagery (Ferreira et al., 2009), higher resolution (0.1 m) should allow for better categorizing the seagrass cover than 0.5 m resolution. However, results did not correspond to this assumption, yielding no differences at methodology level. Indeed, higher resolutions do not always increase the classification accuracy, especially when many spectral signatures correspond to one single category to be classified and can hinder the task of delineation of the vegetal canopies (Nagendra and Rocchini, 2008). The higher computational requirements dictated by the increased number of iterations of the process reflects this fact for NAP images. Additionally some differences on water column visibility affected the average accuracy of the methodology.

Sampling conditions

Andrade and Ferreira, 2011 highlighted the possibility of differences when comparing

situations of different relations between leafs length and water column above. The seagrass leafs position may show different degrees of randomness in relative stagnant waters such as the NAP images location, versus more wave-dynamic environments, such as OTP images location (Koch et al., 2006). Because of that, fine scale imagery, is an important approach to better understand the dynamisms at micro-habitat level and time differences along its structure (Banks and Skilleter, 2007; Dekker et al., 2006). In order to compare 2 different sampling conditions, we focused on to differentiate ranges of tide, emerged versus submerged conditions, and we found that neither OTP (at 0.5 m resolution) nor NAP (at 0.1 m resolution), showed any difference between areas evaluation in each sampling condition (OTP p=0.7527; NAP p=0.9164), which suggests that those issues discussed above, do not affect seagrass coverage evaluations. NAP images were the ones with a larger timeline difference between emerged and submerged conditions. Nonetheless the results showed that this issue did not gave significant differences between both conditions in terms of seagrass distribution.

In addition, results showing no statistical differences between classification accuracies (p=0.1797) when comparing different conditions (Fig. 18), provided an other argument together with the area variation results (no statistical differences either), proving that tide level (within limit of 0.8 m HZ) do not affect image analysis of seagrass meadows limits. Furthermore, for kappa analysis between binary maps comparisons for each pair of images, there is not significant difference between classification at different sampling conditions.

Image classification

When high resolution (either 0.5 or 0.1 m) images are used, each target item (seagrass) is composed of many pixels with a large range of spectral signatures. Furthermore, other not target image items, might have similar spectral signature composition or cover the target (e.g. turbidity). For the reclassification following a pixel-based classification, this can lead the analyst to chose between reclassifying some undesirable items as a target or some desirable items as no target, yielding final maps with salt and pepper effects (e.g., Fig. 14) and mistaken reclassifications, since this classification approach uses only spectral signature grouping criteria. Object-based classification on the other hand (e.g., Fig. 13), allows for the reclassification of individual segments (or objects) without influence to others and produces cleaner classified images (e.g., Fig. 14), since it uses not only spectral signature criteria but contiguity as well. As other authors noticed (Aplin and Smith, 2011; Dupuy et al., 2012;

Hölbling et al., 2012; Klemas, 2013; Lucieer, 2008) in our research, an object-based approach largely and significantly

(p=3.221×10^{-05}) solved the pixel-based limitations. However, in this context, we need to highlight that applying the object-based approach, often produced a more arduous reclassification process than with the pixel-based approach, namely, because the larger number of objects to be reclassified. Nevertheless an affordable drawback given the better classification accuracy results (Fig. 19).

Finally kappa analysis results, seems initially to disagree with some of the results commented above regarding classification accuracies. For instance, it could have been expected to obtain significant higher kappa values between object-based comparisons within same pair of images compared, however, higher values appeared always between pixel and object comparisons from the same sampling condition (Fig. 20). In fact that happened because the following factors combined:

- Georectification process produces certain errors that differ between images and therefore, each image has different geometric correction features (Ferreira et al., 2009; Lu and Weng, 2007). When comparing different classifications approaches (pixel/object) from the same exact image, differences are exclusively due to the classification process. On the other hand, when the comparison includes different conditions (emerged/submerged), means that occurs between different images. Therefore, they are not perfectly overlapped due to the differences on the acquisition and georegistration, giving bigger differences on the classified maps comparisons (Fig. 20). This is more evident on the balloon methodology, due to the georectification issues discussed before.

- Classification accuracies did not differ significantly between emerged and submerged conditions. However, were assessed individually for each map produced. When comparing pairs of thematic maps, the small variability between them due to water visibility, can lead to the observed discrepancies (Foody, 2008, 2002).

Nevertheless the kappa results reported an expected result. Namely the fact that, besides the issues above, the other comparison that scored higher kappa values in both methodologies, is between object-based classifications within different conditions. This, reinforces the argument that it is a better choice to solve eventual visibility differences, allowing for a wider range of

conditions to sample. This result can provide a step forward to Roelfsema et al., 2014 conclusions regarding the need for testing visibility differences for high spatial resolution mapping of seagrass beds.

5 CONCLUSIONS AND FUTURE WORK

Despite the fact that some weather and hydrological limitations need to be considered, NAP methodology allowed for the independence from fixed platforms that are not always available. Furthermore, high resolution images taken at nadir and low altitude from the balloon, produced images with lower less geometric distortion and with higher resolution (more detail) than the ones obtained with the compared methodology proposed by Andrade and Ferreira, 2011 and, therefore, more information on the coverage and heterogeneity of target seagrass beds. Therefore, we can conclude that the proposed low-cost methodology, clearly overcome most of the issues referred for other approaches for ecological mapping purposes.
Furthermore, regarding the sampling conditions, our results can help to optimize future field work decisions, since no significant differences between different tides ranges (within the limit of 0.8 m ZH) were found for mapping seagrass meadows.
Finally, at image classification level, object-based classification approach resulted in a better option to outperform the issues pertaining to turbidity or to the classification of undesirable objects, providing significantly better classification accuracies for both OTP and NAP methodologies.

The results of our study offer a new approach for mapping not only seagrass meadows, but benthic intertidal and shallow subtidal ecosystems in general. The accuracy of the results, together with the ease of use of the methodology and the possibilities of regularly implementing it, provide a tool for better understanding the complexity of those ecosystems and their evolution with a non intrusive approach. An increasingly need in view of their unprecedented fast degradation.

Given the novelty of the methodology and the different variables tested, future work in a longer timeline research should contribute to consolidate these results and to improve the

methodology to allow a wider range of its implementation. Furthermore, despite present results, pixel-based classification approaches shouldn't be set aside, since other objectives, such as mapping biodiversity besides limits, distribution and density of communities, may be better attained through integration of different classification approaches.

Also, a better understanding of the effects of water transparency in classification results is needed to allow for a more accurate guide to optimize field work decisions. Finally, similar studies could be conducted to map other communities to demonstrate the accuracy of this method at different locations and conditions and extend the application of low cost methodologies for ecological research.

6 REFERENCES

Andrade, F., Ferreira, M.A., 2011. A method for monitoring shallow seagrass meadows (*Zostera* spp.) using terrestrial oblique large-scale photography. Aquat. Bot. 95, 103–109.

Aplin, P., Smith, G.M., 2011. Introduction to object-based landscape analysis. Int. J. Geogr. Inf. Sci. 25, 869–875.

Baker, A.K.M., Fitzpatrick, R.W., Koehne, S.R., 2004. High Resolution Low Altitude Aerial Photography for Recording Temporal Changes in Dynamic Surficial Environments. Regolith 21–25.

Banks, S.A., Skilleter, G.A., 2007. The importance of incorporating fine-scale habitat data into the design of an intertidal marine reserve system. Biol. Conserv. 138, 13–29.

Banman, C., 2002. Supervised and Unsupervised Land Use Classification. The Advanced Image Processing Class at Emporia State University (No. ES775). Emporia, USA.

Bendell, L.I., Wan, P.C.Y., 2011. Application of aerial photography in combination with GIS for coastal management at small spatial scales: A case study of shellfish aquaculture. J. Coast. Conserv. 15, 417–431.

Benz, U.C., Hofmann, P., Willhauck, G., Lingenfelder, I., Heynen, M., 2004. Multi-resolution, object-oriented fuzzy analysis of remote sensing data for GIS-ready information. ISPRS J. Photogramm. Remote Sens. 58, 239–258.

Boyle, S.A., Kennedy, C.M., Torres, J., Colman, K., Pérez-Estigarribia, P.E., De La Sancha, N.U., 2014. High-resolution satellite imagery is an important yet underutilized resource in conservation biology. PLoS One 9.

CHDK, 2007. CHDK 1.3.0 Software and Online User Manual [WWW Document]. Download URL http://chdk.wikia.com/wiki/CHDK_User_Manual (accessed March 21st 2014).

Cohen, J., 1960. A coefficient of agreement for nominal scales. Educ. Psycological Meas. 20, 37–46.

Congalton, R.G., 1991. A review of assessing the accuracy of classifications of remotely sensed data. Remote Sens. Environ. 37, 35–46.

Cunha, A.H., Assis, J., Serrão, E.A., 2009. Estimation of available seagrass meadow area in Portugal for transplanting purposes. J. Coast. Res. 2, 1100–1104.

Cunha, A.H., Assis, J.F., Serrão, E. a., 2013. Seagrasses in Portugal: A most endangered marine habitat. Aquat. Bot. 104, 193–203.

Dekker, A., Brando, V., Anstee, J., Fyfe, S., Malthus, T., Karpouthli, E., 2006. Remote Sensing of Seagrass Ecosystems: Use of Spaceborne and Airborne Sensors Arnold, in: A.W.D.Larkum et al. (Eds.), Seagrasses: Biology, Ecology and Conservation. Springer, Dordrecht, 347–359.

Dogan, O.K., Akyurek, Z., Beklioglu, M., 2009. Identification and mapping of submerged plants in a shallow lake using quickbird satellite data. J. Environ. Manage. 90, 2138–2143.

Doxaran, D., Froidefond, J.M., Castaing, P., Babin, M., 2009. Dynamics of the turbidity maximum zone in a macrotidal estuary (the Gironde, France): Observations from field and MODIS satellite data. Estuar. Coast. Shelf Sci. 81, 321–332.

Duarte, C.M., Chiscano, C.L., 1999. Seagrass biomass and production: A reassessment. Aquat. Bot. 65, 159–174.

Duarte, C.M., Fourqurean, J.W., Krause-Jensen, D., Olesen, B., 2006. Dynamics of Seagrass Stability and Change, in: A.W.D.Larkum et al. (Eds.), Seagrasses: Biology, Ecology and Conservation. Springer, Dordrecht, 271–294.

Duarte, C.M., Kirkman, H., 2001. Methods for the measurement of seagrass abundance and depth distribution, in: Short, F.T., Coles, R.C. (Eds.), Global Seagrass Research Methods. Elsevier B.V., 141–154.

Dupuy, S., Barbe, E., Balestrat, M., 2012. An Object-Based Image Analysis Method for Monitoring Land Conversion by Artificial Sprawl Use of RapidEye and IRS Data. Remote Sens. 4, 404–423.

Enslin, W.R., 2011. GRASS GIS manual: i.rectify [WWW Document]. URL ftp://ftp.rz.uni-wuerzburg.de/pub/other/grass/grass65/manuals/html65_user/i.rectify.html (accessed October 9th 2014).

Fabricius, K.E., De'ath, G., Humphrey, C., Zagorskis, I., Schaffelke, B., 2013. Intra-annual variation in turbidity in response to terrestrial runoff on near-shore coral reefs of the

Great Barrier Reef. Estuar. Coast. Shelf Sci. 116, 57–65.

Ferreira, M.A., Andrade, F., Bandeira, S.O., Cardoso, P., Nogueira Mendes, P., Paula, J., 2009. Analysis of cover change (1995–2005) of Tanzania/Mozambique trans-boundary mangroves using Landsat imagery. Aquat. Conserv. Mar. Freshw. Ecosyst. 19, 38–45.

Field, A., Miles, J., Field, Z., 2012. Discovering statistics using R. SAGE Publications Ltd.

Finkbeiner, M., Stevenson, B., Seaman, R., 2001. Guidance for Benthic Habitat Mapping: An Aerial Photographic Approach, National Oceanic and Atmospheric Administration. Charleston, S.C.

Fonseca, M.S., Bell, S.S., 1998. Influence of physical settings on seagrass landscapes near Beaufort, North Carolina, USA. Mar. Ecol. Prog. Ser. 171, 109–121.

Foody, G.M., 2002. Status of land cover classification accuracy assessment. Remote Sens. Environ. 80, 185–201.

Foody, G.M., 2008. Harshness in image classification accuracy assessment. Int. J. Remote Sens. 29, 3137–3158.

Frederiksen, M., Krause-Jensen, D., Holmer, M., Laursen, J.S., 2004. Spatial and temporal variation in eelgrass (*Zostera marina*) landscapes: influence of physical setting. Aquat. Bot. 78, 147–165.

Gacia, E., Granata, T.., Duarte, C.., 1999. An approach to measurement of particle flux and sediment retention within seagrass (*Posidonia oceanica*) meadows. Aquat. Bot. 65, 255–268.

Gillespie, T.W., Foody, G.M., Rocchini, D., Giorgi, A.P., Saatchi, S., 2008. Measuring and Modelling Biodiversity from Space. Prog. Phys. Geogr. 32, 203–221.

GRASS Development Team, 2015. Geographic Resources Analysis Support System (GRASS) Software, Version 7.0. Open Source Geospatial Found. Download URL http://grass.osgeo.org.

Grenzdörffer, G.J., Guretzki, M., Friedlander, I., 2008. Photogrammetric image acquisition and image analysis of oblique imagery. Photogramm. Rec. 23, 372–386.

Hashim, M., Misbari, S., Yahya, N.N., Ahmad, S., Reba, N., Komatsu, T., 2014. An approach for quantification of submerged seagrass biomass in shallow turbid coastal waters, in: Geoscience and Remote Sensing Symposium (IGARSS), 2014 IEEE International. IEEE, Quebec City, 4439–4442.

Heck, K.L., Hays, G., Orth, R.J., 2003. Critical evaluation of the nursery role hypothesis for seagrass meadows. Mar. Ecol. Ser. 253, 123–136.

Hill, V.J., Zimmerman, R.C., Bissett, W.P., Dierssen, H., Kohler, D.D.R., 2014. Evaluating Light Availability, Seagrass Biomass, and Productivity Using Hyperspectral Airborne Remote Sensing in Saint Joseph's Bay, Florida. Estuaries and Coasts 37, 1467–1489.

Hladik, C., Alber, M., 2012. Accuracy assessment and correction of a LIDAR-derived salt marsh digital elevation model. Remote Sens. Environ. 121, 224–235.

Hölbling, D., Füreder, P., Antolini, F., Cigna, F., Casagli, N., Lang, S., 2012. A Semi-Automated Object-Based Approach for Landslide Detection Validated by Persistent Scatterer Interferometry Measures and Landslide Inventories. Remote Sens. 4, 1310–1336.

Hornik, V., 2015. Windguru [WWW site]. URL www.windguru.cz (accessed weekly from September 2014 to August 2015).

Hovel, K.A., Lipcius, R.N., 2001. Habitat Fragmentation in a Seagrass Landscape : Patch Size and Complexity Control Blue Crab Survival. Ecology 82, 1814–1829.

Huth, J., Kuenzer, C., Wehrmann, T., Gebhardt, S., Tuan, V.Q., Dech, S., 2012. Land Cover and Land Use Classification with TWOPAC: towards Automated Processing for Pixel- and Object-Based Image Classification. Remote Sens. 4, 2530–2553.

IH, 2014. Tabelas de maré 2014, Instituto Hidrografico.

IH, 2015. Tabelas de maré 2015, Instituto Hidrografico.

Jensen, J.R., 2005. Introductory digital image processing: a remote sensing perspective, 3rd ed. Prentice Hall, USA.

Kamal, M., Phinn, S., 2011. Hyperspectral Data for Mangrove Species Mapping: A Comparison of Pixel-Based and Object-Based Approach. Remote Sens. 3, 2222–2242.

Kawamura, K., Skuno, Y., Tanaka, Y., Lee, H.-J., Lim, J., Kurokawa, Y., Watanabe, N., 2011. Mapping herbage biomass and nitrogen status in an Italian ryegrass (Lolium multiflorum L.) field using a digital video camera with balloon system. J. Appl. Remote Sens. 5, 1931–3195.

Klemas, V., 2013. Remote sensing of emergent and submerged wetlands: an overview. Int. J. Remote Sens. 34, 6286–6320.

Koch, E.W., Ackerman, J.D., Verduin, J., Van Keulen, M., 2006. Fluid Dynamics in Seagrass Ecology—from Molecules to Ecosystems, in: A.W.D.Larkum et al. (Eds.), Seagrasses: Biology, Ecology and Conservation. Springer, Dordrecht, 193–225.

Koh, L.P., Wich, S.A., 2012. Dawn of drone ecology : low-cost autonomous aerial vehicles for conservation. Trop. Conserv. Sci. 5, 121–132.

Kruskal, W.H., Wallis, W.A., 1952. Use of Ranks in One-Criterion Variance Analysis. J. Am. Stat. Assoc. 47, 583–621.

Kutser, T., Vahtmae, E., Roelfsema, C., Metsamaa, L., 2007. Photo-library method for mapping seagrass biomass. Estuar. Coast. Shelf Sci. 75, 559–563.

Leica Geosystems AG, 2012. User's manual of Leica System GPS, CS15/GS15 field controller. Leica Geosystems AG. Heerbrug, Switzerland

Lonneville, B., De Roo, B., Stal, C., De Wit, B., De Wulf, A., De Maeyer, P., 2013. Accurate and Cost-Efficient 3D Modelling using Motorized Hexacopter, Helium Balloons and Photo Modelling : a Case Study, in: M. Ioannides et al., (Eds.), Lecture Notes in Computer Science. Springer International Publishing Switzerland, 410–417.

Lonneville, B., Stal, C., Roo, B. De, Wit, B. De, Wulf, A. De, Maeyer, P. De, Krijgslaan, S., Stal, C., Deroo, B., Dewit, B., Dewulf, A., Demaeyer, P., Vi, C., Vi, W.G., 2014. HELIUM BALLOONS FOR 3D MODELLING : OFF TO A FLYING START ?, in: Low Cost 3D. Ghent.

Lu, D., Weng, Q., 2007. A survey of image classification methods and techniques for improving classification performance. Int. J. Remote Sens. 28, 823–870.

Lucieer, V.L., 2008. Object-oriented classification of sidescan sonar data for mapping benthic marine habitats. Int. J. Remote Sens. 29, 905–921.

Lyons, M.B., Phinn, S.R., Roelfsema, C.M., 2012. Long term land cover and seagrass mapping using Landsat and object-based image analysis from 1972 to 2010 in the coastal environment of South East Queensland, Australia. ISPRS J. Photogramm. Remote Sens. 71, 34–46.

Macleod, R.D., Congalton, R.G., 1998. A Quantitative comparison of change-detection algorithms for monitoring eelgrass from remotely sensed data. Photogramm. Eng. Remote Sensing 64, 207–216.

Marbà, N., Holmer, M., Gacia, E., Barrón, C., 2006. Seagrass Beds and Coastal Biogeochemistry, in: A.W.D.Larkum et al. (Eds.), Seagrasses : Biology, Ecology and Conservation. Springer, Dordrecht, 135–157.

Mohammed, N.Z., Eisa Eiman, A.E., 2013. The Effect of Polynomial Order on Georeferencing Remote Sensing Images. Int. J. Eng. Innov. Technol. 2, 5–8.

Momsen, E., Metz, M., 2015. GRASS GIS manual: i.segment [WWW Document]. URL https://grass.osgeo.org/grass70/manuals/i.segment.html (accessed February 13th 2015).

Montané, J.M., Torres, R., 2006. Accuracy Assessment of Lidar Saltmarsh Topographic Data Using RTK GPS. Photogramm. Eng. Remote Sens. 72, 961–967.

Moore, K.A., Short, F.T., 2006. Zostera: Biology, Ecology, and Management, in: A.W.D.Larkum et al. (Eds.), Seagrasses: Biology, Ecology and Conservation. Springer, Dordrecht, 361–386.

Muise, A., 2010. Raster Image Processing Tips and Tricks — Part 2: Mosaicking [WWW Document]. ArcGis Resour. URL http://blogs.esri.com/esri/arcgis/2010/10/26/georef2/ (accessed March 11th 2015).

Nagendra, H., Rocchini, D., 2008. High resolution satellite imagery for tropical biodiversity studies: the devil is in the detail. Biodivers. Conserv. 17, 3431–3442.

Nayak, S., Behera, M.D., 2009. Improving Land-Use and Vegetation Cover Classification Accuracy using Fuzzy Logic - A Study in Pilibhit District, Uttar Pradesh, India. Int. J. Geoinformatics 5, 1–10.

Neteler, M., Bowman, M.H., Landa, M., Metz, M., 2012. GRASS GIS: A multi-purpose open source GIS. Environ. Model. Softw. 31, 124–130.

Neteler, M., Mitasova, H., 2008. Open source GIS, a GRASS GIS approach, 3rd ed. Springer Science+Business Media, LLC.

Orth, R.J., Carruthers, T.J.B., Dennison, W.C., Duarte, C.M., Fourqurean, J.W., Heck JR., K.L., Hughes, A.R., Kendrick, G.A., Kenworthy, W.J., Olyarnik, S., Short, F.T., Waycott, M., Williams, S.L., 2006. A global crisis for seagrass ecosystems. Bioscience 56, 987–996.

Phinn, S., Roelfsema, C., Dekker, A., Brando, V., Anstee, J., 2008. Mapping seagrass species, cover and biomass in shallow waters: An assessment of satellite multi-spectral and airborne hyper-spectral imaging systems in Moreton Bay (Australia). Remote Sens. Environ. 112, 3413–3425.

QGIS Development Team, 2009. QGIS Geographic Information System. Open Source Geospatial Found. Download URL http://qgis.osgeo.org.

R Core Development Team, 2008. R: A language and environment for statistical computing. [WWW Document]. R Found. Stat. Comput. Vienna, Austria. Download URL http://www.r-project.org (accessed March 13th 2015).

Rocchini, D., Metz, M., Frigeri, A., Delucchi, L., Marcantonio, M., Neteler, M., 2011. Robust rectification of aerial photographs in an open source environment. Comput. Geosci. 39, 145–151.

Roelfsema, C.M., Lyons, M., Kovacs, E.M., Maxwell, P., Saunders, M.I., Samper-Villarreal, J., Phinn, S.R., 2014. Multi-temporal mapping of seagrass cover, species and biomass: A semi-automated object based image analysis approach. Remote Sens. Environ. 150, 172–187.

Shapiro, M., 2012a. GRASS GIS manual: i.cluster [WWW Document]. URL https://grass.osgeo.org/grass64/manuals/i.cluster.html (accessed February 3rd 2015).

Shapiro, M., 2012b. GRASS GIS manual: i.maxlik [WWW Document]. URL https://grass.osgeo.org/grass64/manuals/i.maxlik.html (accessed February 3rd 2015).

Silva, T.S.F., Costa, M.P.F., Melack, J.M., Novo, E.M.L.M., 2008. Remote sensing of aquatic vegetation: theory and applications. Environ. Monit. Assess. 140, 131–45.

Silveira, T.M., Kraus, N.C., Psuty, N.P., Andrade, F., 2011. Beach Nourishment on Troia Peninsula, Portugal. J. Coast. Res. 59, 173–180.

Su, H., Karna, D., Fraim, E., Fitzgerald, M., Dominguez, R., Myers, J.S., Coffland, B.,

Handley, L.R., Mace, T., 2006. Evaluation of Eelgrass Beds Mapping Using a High-Resolution Airborne Multispectral Scanner. Photogramm. Eng. Remote Sens. 72, 789–797.

Thomson, A.G., 1998. Supervised versus unsupervised methods for classification of coasts and river corridors from airborne remote sensing. Int. J. Remote Sens. 19, 3423–3431.

Turner, D., Lucieer, A., Watson, C., 2012. An automated technique for generating georectified mosaics from ultra-high resolution Unmanned Aerial Vehicle (UAV) imagery, based on Structure from Motion (SFM) point clouds. Remote Sens. 4, 1392–1410.

Urbański, J.A., Mazur, A., Janas, U., 2009. Object-oriented classification of QuickBird data for mapping seagrass spatial structure. Oceanol. Hydrobiol. Stud. 38, 27–43.

Vo, Q.T., Oppelt, N., Leinenkugel, P., Kuenzer, C., 2013. Remote sensing in mapping mangrove ecosystems - an object-based approach. Remote Sens. 5, 183–201.

Wang, L., Sousa, W.P., Gong, P., 2004. Integration of object-based and pixel-based classification for mapping mangroves with IKONOS imagery. Int. J. Remote Sens. 25, 5655–5668.

Waycott, M., Duarte, C.M., Carruthers, T.J.B., Orth, R.J., Dennison, W.C., Olyarnik, S., Calladine, A., Fourqurean, J.W., Heck, K.L., Hughes, A.R., Kendrick, G.A., Kenworthy, W.J., Short, F.T., Williams, S.L., 2009. Accelerating loss of seagrasses across the globe threatens coastal ecosystems. Proc. Natl. Acad. Sci. U. S. A. 106, 12377–12381.

Wen, T., 2014. GRASS GIS manual: r.kappa [WWW Document]. URL https://grass.osgeo.org/grass64/manuals/r.kappa.html (accessed February 22nd 2015).

Yan, G., Mas, J. −F., Maathuis, B.H.P., Xiangmin, Z., Van Dijk, P.M., 2006. Comparison of pixel−based and object−oriented image classification approaches—a case study in a coal fire area, Wuda, Inner Mongolia, China. Int. J. Remote Sens. 27, 4039–4055.

Zharikov, Y., Skilleter, G.A., Loneragan, N.R., Taranto, T., Cameron, B.E., 2005. Mapping and characterising subtropical estuarine landscapes using aerial photography and GIS for potential application in wildlife conservation and management. Biol. Conserv. 125, 87–100.

Zimmerman, R.C., Dekker, A.G., 2006. Aquatic Optics: Basic Concepts for Understanding How Light Affects Seagrasses and Makes them Measurable from Space, in: A.W.D.Larkum et al. (Eds.), Seagrasses: Biology, Ecology and Conservation. Springer, Dordrecht, 295–301.